

# Water Resources Research

## RESEARCH ARTICLE

10.1029/2023WR035547

### Key Points:

- Wine industry residues induced nitrate attenuation in laboratory batch and column experiments
- Denitrification efficiency varied with the wine residue type, showing  $\epsilon^{15}\text{N}$  between  $-16.5$ – $-32.0\text{‰}$  and  $\epsilon^{18}\text{O}$  between  $-12.1$ – $-27.6\text{‰}$
- A geochemical model describing the trends of the experimental results has been developed and can be used for field applications

### Supporting Information:

Supporting Information may be found in the online version of this article.

### Correspondence to:

A. Abu,  
[alexabu@ub.edu](mailto:alexabu@ub.edu)

### Citation:

Abu, A., Carrey, R., Navarro-Ciurana, D., Margalef-Martí, R., Soler, A., Otero, N., et al. (2024). Enhancing nitrate removal with industrial wine residue: Insights from laboratory batch and column experiments using chemical, isotopic and numerical modeling tools. *Water Resources Research*, 60, e2023WR035547. <https://doi.org/10.1029/2023WR035547>

Received 15 JUN 2023

Accepted 24 APR 2024

### Author Contributions:

**Conceptualization:** Raúl Carrey, Cristina Domènech

**Data curation:** Alex Abu

**Formal analysis:** Alex Abu

**Funding acquisition:** Albert Soler, Neus Otero

**Methodology:** Alex Abu, Raúl Carrey, Dídac Navarro-Ciurana, Cristina Domènech






**Supervision:** Dídac Navarro-Ciurana, Cristina Domènech

**Validation:** Alex Abu, Raúl Carrey, Dídac Navarro-Ciurana, Cristina Domènech

© 2024. The Authors.

This is an open access article under the terms of the [Creative Commons Attribution-NonCommercial-NoDerivs License](https://creativecommons.org/licenses/by/4.0/), which permits use and distribution in any medium, provided the original work is properly cited, the use is non-commercial and no modifications or adaptations are made.

## Enhancing Nitrate Removal With Industrial Wine Residue: Insights From Laboratory Batch and Column Experiments Using Chemical, Isotopic and Numerical Modeling Tools

Alex Abu<sup>1,2</sup> , Raúl Carrey<sup>2,3</sup>, Dídac Navarro-Ciurana<sup>1,2</sup>, Rosanna Margalef-Martí<sup>1,2</sup> , Albert Soler<sup>1,2</sup>, Neus Otero<sup>1,2,4</sup> , Jesús Causapé<sup>5</sup> , and Cristina Domènech<sup>1,2</sup> 

<sup>1</sup>Grup MAiMA, Mineralogia Aplicada, Geoquímica i Hidrogeologia—MAGH, Departament de Mineralogia, Petrologia i Geologia Aplicada, Facultat de Ciències de La Terra, Universitat de Barcelona (UB), Barcelona, Spain, <sup>2</sup>Institut de Recerca de l'Aigua (IdRA), Universitat de Barcelona (UB), Barcelona, Spain, <sup>3</sup>Centres Científics i Tecnològics, Universitat de Barcelona (UB), Barcelona, Spain, <sup>4</sup>Serra Hünter Fellowship, Generalitat de Catalunya, Catalonia, Spain, <sup>5</sup>Geological and Mining Institute of Spain—IGME, Zaragoza, Spain

**Abstract** Agricultural run-off exposes recipient water bodies to nitrate ( $\text{NO}_3^-$ ) pollution. Biological denitrification is a suitable method for removing  $\text{NO}_3^-$  in water resources that can be induced by the use of industrial organic liquid waste as an electron donor source. In light of this, batch and column laboratory experiments were performed to assess the potential of two industrial wine residues (*lías* and *vínico*) to induce biological denitrification of  $\text{NO}_3^-$  contaminated water from a constructed wetland and to evaluate the efficiency of these treatments using chemical and isotopic tools. In batch experiments (performed at a C/N ratio of 1.25), *vínico* was not efficient enough in removing N species, attenuating only 35%  $\text{NO}_3^-$  and was not used in column experiments. In similar experimental conditions, *lías* completely removed N species from water in both batch and column experiments. The calculated isotope fractionation ( $\epsilon^{15}\text{N}_{\text{NO}_3}$  and  $\epsilon^{18}\text{O}_{\text{NO}_3}$ ) was the same in both batch and column experiments biostimulated with *lías* and differed from those for *vínico*. The isotopic data confirmed that denitrification was the principal  $\text{NO}_3^-$  attenuation pathway in all the experiments. The isotopic fractionation can be later applied to field studies to quantify the efficiency of biologically enhanced denitrification. A numerical geochemical model that accounts for the changes in nitrate, nitrite concentration and isotopic composition due to the degradation of *lías* and *vínico*, including transport in the case of the column experiment, was performed to simulate the experimental results and can be up-scaled in field treatments.

**Plain Language Summary** Groundwater nitrate pollution is a significant global concern resulting from excessive fertilizer use in agriculture. This pollution poses health risks to humans and ecosystems by contaminating drinking water supplies and aquatic ecosystems. Sustainable remediation of nitrate is necessary to safeguard human health and the environment. Successful field-scale remediation requires laboratory feasibility studies to find the appropriate compounds to reduce nitrate (electron donors) and the best application measures to remove nitrate at a minimum cost. In our research, laboratory experiments were carried out using two industrial wine wastes as electron donors to evaluate their potential to remove nitrate from nitrate-polluted water. Chemical, isotopic, and numerical modeling tools have been used to quantify the amount of nitrate removed. The results indicate that one product successfully removed nitrate and can be implemented in the field as a mitigation strategy, while the other was ineffective and cannot be used. The isotopic fractionation from the laboratory experiments and the numerical model would be subsequently applied in the field to quantify the efficiency of nitrate removal.

## 1. Introduction

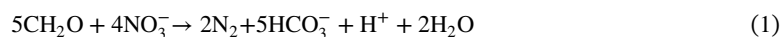
Nitrogen from anthropogenic activities has been identified as one of the primary constituents of agricultural run-off and municipal and industrial wastewater (Lu et al., 2009). Leachates of N from these sources are oxidized to nitrate ( $\text{NO}_3^-$ ) in aerobic conditions. In many agricultural areas,  $\text{NO}_3^-$  is a common water resources pollutant that poses a significant challenge because elevated  $\text{NO}_3^-$  concentrations may cause environmental impacts such as eutrophication, harmful algal blooms, and associated human health hazards such as stomach cancer and blue-baby syndrome (WHO, 2017). To render water safe for human consumption, the European Union Nitrate Directive established a  $\text{NO}_3^-$  concentration threshold value of  $50 \text{ mg NO}_3^- \text{ L}^{-1}$  (WHO, 2017). Many agricultural basins

**Writing – original draft:** Alex Abu  
**Writing – review & editing:** Raúl Carrey,  
Dídac Navarro-Ciurana,  
Rosanna Margalef-Martí, Albert Soler,  
Neus Otero, Jesús Causapé,  
Cristina Domènech

globally have recorded  $\text{NO}_3^-$  concentrations above this limit. The treatment of agricultural run-off before discharging it into the environment is essential to reduce  $\text{NO}_3^-$  loads in receiving water bodies.

Constructed Wetlands (CWs) are horizontal-flow artificial ponds specially designed to remediate wastewater in a controlled environment and are often used to treat agricultural run-off and industrial and municipal wastewater. Numerous studies have demonstrated the potential of CWs to efficiently remediate N-rich ( $\text{NO}_3^-$ ,  $\text{NO}_2^-$ , and  $\text{NH}_4^+$ ) wastewaters. CWs are easy to operate and cost-effective, with generally low capital and operational expenses (Phipps & Crumpton, 1994; Wu et al., 2014). As agricultural/municipal/industrial wastewater is directed to and flows through CWs, N is transformed through processes such as plant uptake, nitrification, denitrification, dissimilatory nitrate reduction to ammonia (DNRA), and/or anaerobic ammonium oxidation (anammox) (Figure 1) (Picardal, 2012; Sebilo et al., 2006). While denitrification and anammox remove N from wastewater as gaseous products, nitrification and DNRA only change the N form (Figure 1). The impact of seasonal temperature, N loading capacity, dissolved oxygen ( $\text{O}_2$ ) transfer, organic matter source and quantity, microbial species, wetland age, and hydraulic retention time play critical roles in N attenuation efficiency (Carrey et al., 2014; Grau-Martínez et al., 2017; Valhondo et al., 2020).

Even though all the aforementioned N cycling pathways can take place in CWs, denitrification is considered the main N removal process (Saeed & Sun, 2017), which reduces  $\text{NO}_3^-$  to  $\text{N}_{2(g)}$  through intermediate steps driven by denitrifying bacteria (Figure 1). Bacteria responsible for N species transformations are abundant in surface and subsurface waters (Beauchamp et al., 1989).  $\text{NO}_3^-$  reductase bacteria are primarily facultative anaerobic denitrifying heterotrophs that oxidize organic compounds to generate energy for growth and cell synthesis (Reaction 1). Anaerobic biological denitrification occurs with oxygen concentration below  $2 \text{ mg L}^{-1}$  (Singleton et al., 2007).



Denitrification efficiency in many CWs is less than 50% due to the limitation of organic matter (Li et al., 2014; Torrijos et al., 2016). To improve the removal of  $\text{NO}_3^-$  in CWs, the biologically enhanced denitrification (BED) approach is adopted to provide external organic matter as a source of electron donors.

In long-term nitrate remediation treatments, using pure organic carbon sources such as glucose, acetate, ethanol and methanol could be costly (Margalef-Martí, Carrey, Merchán, et al., 2019). Therefore, the concept of the circular economy offers an optimal solution by transforming waste products into valuable resources. Industrial residues provide an alternative cheap and easily accessible electron donor source aligning with the principles of the circular economy. Various organic matter sources, including whey (Margalef-Martí, Carrey, Soler, & Otero, 2019), plant-based compost and woodchips (Grau-Martínez et al., 2017; Valhondo et al., 2020), and glucose (Calderer et al., 2010), have been investigated in micro and meso-scale studies to enhance  $\text{NO}_3^-$  removal.

Nitrogen microbial-mediated reactions tend to alter isotopic distribution in nitrogen compounds, affecting both the substrate and product pools according to the isotopic fractionation factor, which quantifies the relative segregation between the light and heavy isotopes. Because of isotopic fractionation, the heavy isotopes of N and O are enriched during nitrate reduction, providing insights into nitrogen cycling and denitrification efficiency.  $\text{NO}_3^-$  isotopologues aid in tracing nitrate sources and assessing natural and induced denitrification, in contrast to processes such as dilution or mixing between nitrate-polluted water resources and non-polluted waters by  $\text{NO}_3^-$ , which often alter nitrate concentration but do not modify the nitrate isotopic composition, making isotopic tools particularly advantageous in field scale studies (Mariotti et al., 1981). Combining multi-isotopic studies with chemical data is valuable for studying biological denitrification in water resources (Otero et al., 2009).

Numerical modeling tools are valuable for research and investigation, providing a means for synthesizing and interpreting data, evaluating complex processes, testing scenarios, and predicting long-term reactions beyond laboratory experiments (Zhu, 2012). They have been applied to characterize the fate and transport of  $\text{NO}_3^-$  in groundwater, in both laboratory scale (André et al., 2011; Rodríguez-Escales et al., 2014) and field studies (Kildsgaard & Engesgaard, 2001; Kinzelbach et al., 1991). Although  $\text{NO}_3^-$  isotopologues aid in studying groundwater N transformation processes (Carrey et al., 2013; Margalef-Martí, Carrey, Soler, & Otero, 2019), limitations exist in quantifying multiple reactions (Abu et al., 2022). Therefore, combining chemical and isotopic tools with numerical modeling could enhance the understanding of nitrate attenuation processes.

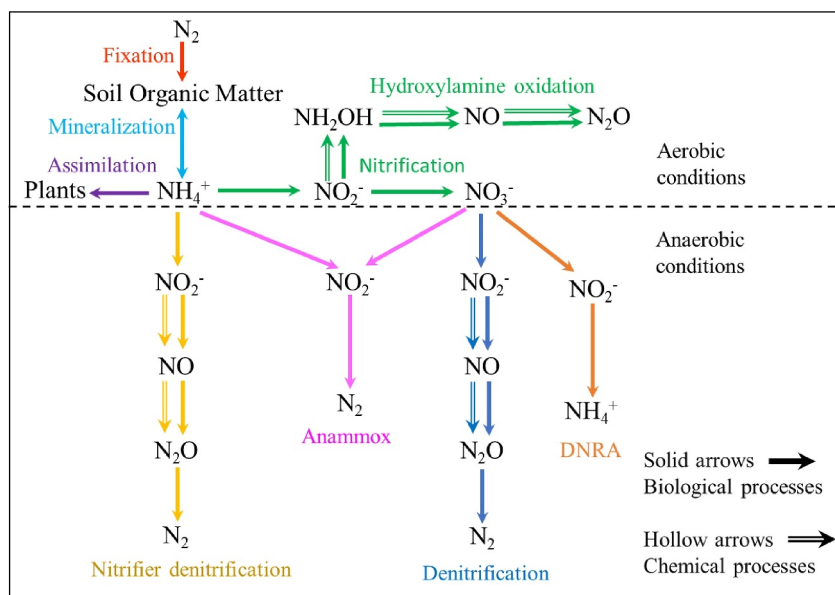


**Figure 1.** A. scheme showing biological and chemical N attenuation pathways in groundwater in aerobic and anaerobic conditions (modified after Abu et al. (2022)).

An example of a N-polluted basin is the Lerma basin, a small catchment area (7.33 km<sup>2</sup>) in northeastern Spain (Zaragoza), located on the left bank of the Ebro River. Over the past two decades, the Lerma basin has been subjected to anthropogenic activities, primarily irrigation agriculture (Abrahamo et al., 2013) and fertilization (Merchán et al., 2015). Agricultural run-off in the Lerma basin has significantly increased N exports to the surrounding water bodies and has caused the principal recipient water body (Arba River) to be polluted with NO<sub>3</sub><sup>-</sup> (Merchán et al., 2015). In 2015, a CW was built in the Lerma basin to remove N before discharge into the environment. Details on the construction and operation of the Lerma Basin CW can be found in Margalef-Marti, Carrey, Merchán, et al. (2019) and Merchán et al. (2015).

Biologically enhanced denitrification through CW application was previously tested on the Lerma basin run-off water into the CW at a laboratory scale using corn stubble, wheat hay, and animal compost to determine their potential to remove NO<sub>3</sub><sup>-</sup>, and a pilot test using corn stubble was tested at field scale (Margalef-Marti, Carrey, Merchán, et al., 2019; Merchán et al., 2015). However, results showed that denitrification was not sustained at high flow rates for long time periods. For example, the application of corn stubble at the field-scale resulted in at least 60% NO<sub>3</sub><sup>-</sup> removal using a flow rate of 16 L s<sup>-1</sup>, but this efficiency was limited to a maximum of 3 months due to the vertical diffusion of O<sub>2</sub>. Therefore, there is a need to characterize other possible organic matter sources and the best treatment strategy to improve their sustainability and increase nitrate removal efficiency.

Industrial wine waste holds considerable promise as a valuable carbon source for advancing research in biological denitrification. Wine residues are cost-effective and align with the circular economy concept by reusing discarded materials. This approach supports the United Nations Sustainable Development Goals (SDGs 6 & 7) related to clean water, waste reduction, and resource efficiency (United Nations, 2022), which are increasingly important in today's research and industrial landscape. The use of wine waste reduces the environmental impact associated with carbon dioxide (CO<sub>2</sub>) and methane (CH<sub>4</sub>) gas emissions during wine waste disposal (Niculescu & Ionete, 2023). Therefore, efficiently processing wine waste as electron donors in denitrification can contribute to diminishing these greenhouse gas emissions (Ioannou et al., 2015). Liquid organic waste from wine residues contains a higher concentration of nutrients, including organic carbon, making it readily available for denitrification processes and potentially accelerating these reactions compared to solid organic waste.

In this context, the aim of this study is to determine the potential of two different industrial wine residues to stimulate biological denitrification at the laboratory scale as they may provide an economically feasible solution to nitrate remediation while providing waste recycling (circular economy) and could be easily applied to field studies. Batch and column laboratory experiments were performed with water from the Lerma basin using

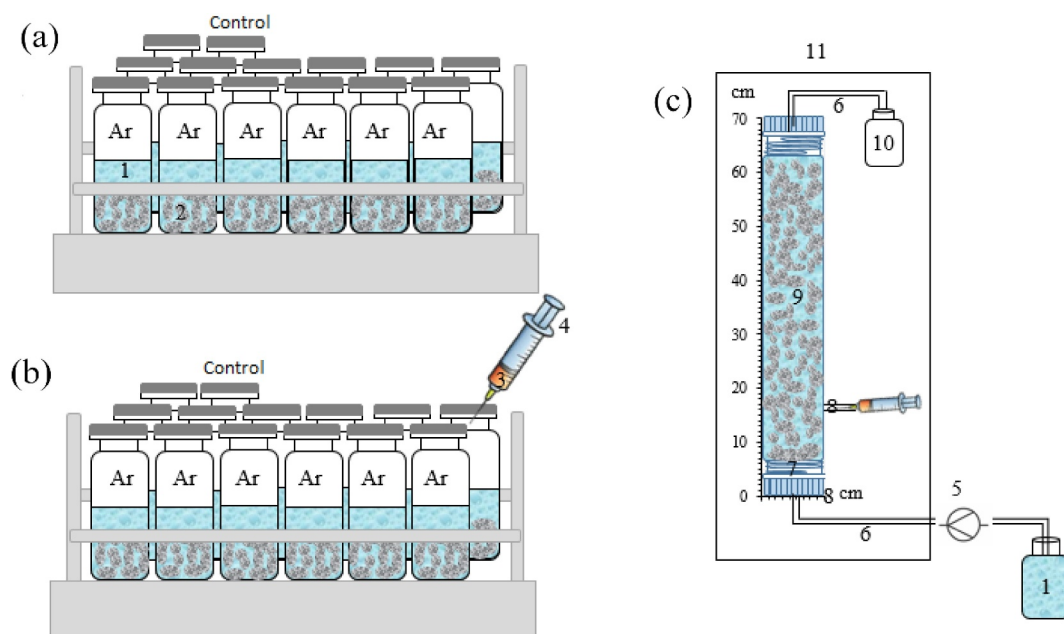


**Figure 2.** A scheme of the experimental set-up: (a) B-L; (b) B-V; (c) C-L with components: 1, field water; 2, gravel material; 3, wine residue; 4, syringe; 5, peristaltic pump; 6, Tygon tubes; 7, silica balls; 8, injection point; 9, glass column; 10, outflow water reservoir; 11, refrigerating chamber. For a more detailed description, see Margalef-Martí, Carrey, Soler, and Otero (2019).

chemical and multi-isotopic tools to quantify the treatment efficiency. Geochemical models describing denitrification processes have received relatively limited attention in scientific research. Therefore, this study also aimed at simulating the evolution of  $\text{NO}_3^-$ ,  $\text{NO}_2^-$ , non-purgeable dissolved organic carbon (NPDOC) concentrations,  $\delta^{15}\text{N}$  and  $\delta^{18}\text{O}$  of  $\text{NO}_3^-$  and  $\text{NO}_2^-$  using numerical models in order to have a verified tool for future field applications and other case studies in similar experimental conditions.

## 2. Materials and Methods

### 2.1. Laboratory Experiments

Batch assays consisted of 250 mL crystal Pyrex® reactors containing 150 mL of field water (FW) and 75 g of gravel material obtained from the CW of the Lerma Basin. Some parts of the CW are covered with gravelly material, providing subsurface flow to limit the vertical diffusion of  $\text{O}_2$ , and the gravel used in the laboratory experiments is used to mimic the field conditions. Field water, in our context, refers to water from the Lerma basin entering the CW that was sampled in 25 L gallons and stored in the fridge at 4°C until use.

The industrial wine wastes were obtained from Destileria San Valero Sociedad Cooperativa Limitada, Cariñena (Spain). The company produces liquid by-products from lees and pomace from 45 partner wineries. The liquid wastes produced during the first and second fermentation in the winemaking process are called “*lías*” and “*vínico*,” respectively. *Lías* and *vínico* were used as electron donor sources to enhance biological denitrification in the experiments. The Total Organic Carbon (TOC) concentration was 20,177.9 and 33,531.1 mg L<sup>-1</sup> in *lías* and *vínico*, respectively.

Two sets of batch experiments (13 samples each) were carried out to test the potential of these two liquid wastes to induce biological denitrification (Figures 2a and 2b). The first set of batch experiments was biostimulated with *lías* and shall be referred to as B-L hereafter. The second set was biostimulated with *vínico* and shall be called B-V hereafter. The reactors were covered with aluminum crimp caps with septa (Figures 2a and 2b) and purged with Ar to remove  $\text{O}_2(\text{g})$  and create an anaerobic environment. Both series of experiments included a control reactor with field water and gravel but with no added waste (Control).

A column experiment was performed to mimic field conditions. The column experiment was biostimulated with *lías*, which shall be called C-L hereafter. In Section 3.1, it is explained why the column experiment was not biostimulated with *vínico*. Field water was pumped from the inflow reservoir through a 70 cm long glass column (8 cm diameter) and discharged into an outflow reservoir by a peristaltic pump (Micropump Reglo digital four channels, ISMATEC) (Figure 2b). The outflow reservoir affixed to the glass column by a Tygon tube was installed in a refrigerating chamber. Similar Tygon tubes connected the glass column to the peristaltic pump and the inflow reservoir (Figure 2b). The top and bottom 2.5 cm of the glass column were filled with 5 mm diameter silica balls to provide homogenous flow at these parts of the glass column, and the remaining glass column was filled with gravel from the CW (volume = 1.6 L) to simulate field conditions by providing a heterogeneous porous media. A constant flow rate of 0.5 mL min<sup>-1</sup> was maintained throughout the experiment. The organic matter source was injected at 16 cm from the bottom of the column daily for 4 days. Afterward, the injection was stopped, allowing NO<sub>3</sub><sup>-</sup> to recover to its initial concentration. Sampling was carried out only at the outflow reservoir. Before the injection of organic carbon into the system, a conservative Cl<sup>-</sup> tracer test was carried out to assess the system performance and determine the hydraulic and transport parameters of the column. Considering this study's scope and objectives, we did not conduct experimental measurements of biomass concentrations or assess the community dynamics of denitrifying bacteria in batch and column experiments.

## 2.2. Analytical Methods

pH, Eh and electrical conductivity were measured using pH, Eh and conductivity meters immediately after sampling. Samples for chemical and isotopic analyses were prepared at the laboratory of the MAiMA-UB research group and analyzed at the Centres Científics i Tecnològics of the Universitat de Barcelona (CCiT-UB). The biostimulated reactors were sequentially sacrificed at specific time intervals based on the denitrification dynamics, while the control reactors were sacrificed at the end of the experiment (the time for sample sacrifice can be found in Tables S2 and S3). Sampled volumes for NPDOC, cations and anions analyses were filtered through a 0.22 μm Millipore® filter, acidified with HCl (for NPDOC analysis) and HNO<sub>3</sub> (for analysis of cations) and stored at +4°C. Dissolved inorganic carbon (DIC) was measured using the titration method (METROHM 702 SM Titrimo). TOC and NPDOC were analyzed using the organic matter combustion method (TOC 500 SHIMADZU). Major cations (Ca, Na, K, and Mg) were analyzed by Inductively Coupled Plasma Optical Emission Spectroscopy (ICP-OES, Perkin-Elmer Optima 8300) and trace elements (Fe, Mn, Si, B, Zn, Co, Cu, Pb, Cd, and Mo) by Inductively Coupled Plasma Mass Spectrometry (ICP-MS, Perkin Elmer NexIon 350D). The concentration of anions NO<sub>3</sub><sup>-</sup>, NO<sub>2</sub><sup>-</sup>, SO<sub>4</sub><sup>2-</sup> and Cl<sup>-</sup> was analyzed by ion chromatography with UV detectors (UV detection limit 214 nm). Samples for δ<sup>15</sup>N-NO<sub>3</sub><sup>-</sup> and δ<sup>18</sup>O-NO<sub>3</sub><sup>-</sup> analyses were kept frozen until analyzed. The nitrogen and oxygen isotopic abundance of dissolved nitrate (δ<sup>15</sup>N-NO<sub>3</sub><sup>-</sup> and δ<sup>18</sup>O-NO<sub>3</sub><sup>-</sup>) were analyzed using the cadmium (Cd) and sodium azide (NaN<sub>3</sub>) reduction methods (McIlvin & Altabet, 2005; Ryabenko et al., 2009). Notations were expressed as δ relative to the international standards (V-SMOW for δ<sup>18</sup>O and Atmospheric N<sub>2</sub> for δ<sup>15</sup>N). The international standards USGS 32, USGS 34 and USGS 35 and the internal laboratory standards, CCiT-IWS-NO3 and CCiT-IWS-NO2, were used to correct the δ<sup>15</sup>N and δ<sup>18</sup>O of NO<sub>3</sub><sup>-</sup> and NO<sub>2</sub><sup>-</sup>, respectively. The wide range of patterns ensures that the values of the analyzed samples fall within the range of pattern values in accordance with the recommendations of the IAEA (Coplen, 2011), thus ensuring the accurate correction of the analytical data. The reference values of these standards and the reproducibilities are presented in Table S1 of the Supporting Information S1.

NO<sub>3</sub><sup>-</sup> attenuation is often characterized by isotope fractionation, controlled by the kinetic isotope effect (Mariotti et al., 1981). In a closed system, the magnitude of fractionation is characterized using the Rayleigh distillation Equation 2, where ε is the kinetic isotope fractionation, C<sub>0</sub> and C<sub>t</sub> are the initial and residual concentration at time zero and t, respectively, and R<sub>0</sub> and R<sub>t</sub> are the isotopic ratios at time zero and t, respectively.

$$\text{Ln}\left(\frac{R_t}{R_0}\right) = \varepsilon \cdot \text{Ln}\left(\frac{C_t}{C_0}\right) \quad (2)$$

The values of R are calculated according to Equation 3, where ε is the isotopic composition (‰).

$$R = \frac{\delta}{1000} + 1 \quad (3)$$



### 2.3. Numerical Modeling Methods

Geochemical calculations and modeling have been carried out with the GibbsStudio software (Nardi & de Vries, 2017) based on PHREEQC version 3 code (Parkhurst & Appelo, 2013) and the iso.dat database.

PHREEQC is a computer program used worldwide for geochemical calculations. PHREEQC can quantify various physical and chemical processes such as aqueous, mineral, gas, solid-solution, surface-complexation, ion-exchange equilibria, kinetically controlled reactions, and one-dimensional transport. The iso.dat database provided with the code used in this study contains data for the simulation of isotopic fractionation of carbon, hydrogen, nitrogen, oxygen, and sulfur (Parkhurst & Appelo, 2013). Equations considered in the models are presented in Supporting Information S1 and in the conceptual model section. GibbsStudio helps to manage water chemistry sample data and run PHREEQC models in a unified productive graphical environment (Nardi & de Vries, 2017).

The coupled microbial reduction of N oxides and the oxidation of organic compounds linked to biomass growth and decay are described using Monod kinetics, alongside changes in nitrate isotopic composition governed by first-order degradation kinetics, are detailed in Section 4 under geochemical modeling. The model-data calibration was performed using CeresStudy within the GibbsStudio environment. This process employed the least-squares curve fitting technique, using the Levenberg–Marquardt algorithm, often referred to as LMA or simply LM, for nonlinear parameter estimation. The selection of the Levenberg–Marquardt algorithm in this study was driven by its robustness, rapid convergence, and versatility (Nardi & de Vries, 2017). Nitrate and nitrite concentrations of the batch experiments were used for the calibration process. In our analysis, the Least Square Error (LSE) is utilized to determine the best-fit line that minimizes the sum of squared differences between observed data points and predicted values.

## 3. Experimental Results and Discussion

### 3.1. Batch Results and Discussion

Chemical data of the field water used in the experiments are summarized in Table S2. Results of the batch experiments with *lías* and *vinico* are summarized in Tables S2 and S3, respectively. In batch experiments, the measured conductivities and pH were constant over time. Conductivities averaged  $2.37 \pm 0.05 \text{ mS cm}^{-1}$  in B-L and  $2.52 \pm 0.01 \text{ mS cm}^{-1}$  in B-V, and pH averaged  $7.85 \pm 0.12$  in B-L and  $7.58 \pm 0.08$  in B-V experiments. Geochemical calculations with the Phreeqc software revealed a constant ionic strength over time.

The concentrations of  $\text{NO}_3^-$ ,  $\text{NO}_2^-$ , and NPDOC for B-L and B-V are shown in Figures 3a and 3b, respectively. In the early stages of batch experiments, wine waste dissolution raised nitrate levels above the inflow water concentration after injecting the organic residue into the batch reactors. Results revealed an essential  $\text{NO}_3^-$  concentration increase from 1.7 to 2.8 mM in B-L and from 1.7 to 2.6 mM in B-V in 12 hr. In the control reactor, changes in  $\text{NO}_3^-$  concentration were not observed over time, indicating that the  $\text{NO}_3^-$  increase was linked to additional  $\text{NO}_3^-$  provided by the wine residues. In the biological denitrification studies with whey, Margalef-Martí, Carrey, Soler, and Otero (2019) and Oliveira et al. (2002) pointed out that industrial liquid wastes could be a potential source of  $\text{NO}_3^-$ , denitrifying bacteria and cations, so wine residues could account for the increased  $\text{NO}_3^-$  concentration in B-L and B-V.

$\text{NO}_3^-$  attenuation in the batch reactors was linked to external organic carbon supplied by the wine wastes. In the B-L experiment,  $\text{NO}_3^-$  attenuation was quick, and  $\text{NO}_3^-$  was completely removed in 2 days (Figure 3a), demonstrating an efficient N removal capacity. The rapid  $\text{NO}_3^-$  attenuation could be explained by the capacity of *lías* to supply organic carbon to the latent denitrifying bacteria of the field water and gravel, which will quickly acclimate upon injection of the wine waste. In B-V,  $\text{NO}_3^-$  slightly decreased from peak  $\text{NO}_3^-$  concentration (2.6–1.1 mM) at the end of the experiment, representing 35%  $\text{NO}_3^-$  removal. Different N attenuation efficiencies were observed in the batch experiments, attributed to the composition of the wine residues used. *Lías* contained highly labile organic carbon content, resulting in high N attenuation in B-L. *Vinico*, on the other hand, mainly contains humic and fulvic acids with less labile organic carbon and, hence, lower efficiency in removing  $\text{NO}_3^-$  (Akunna et al., 1993).

$\text{NO}_3^-$  reduction in B-L was coupled with a slight  $\text{NO}_2^-$  accumulation (up to 0.5 mM) on day one.  $\text{NO}_2^-$  decreased afterward and was below detection ( $<2 \times 10^{-4}$  mM) after day 3 (Figure 3a), while  $\text{NO}_3^-$  reduction in B-V was

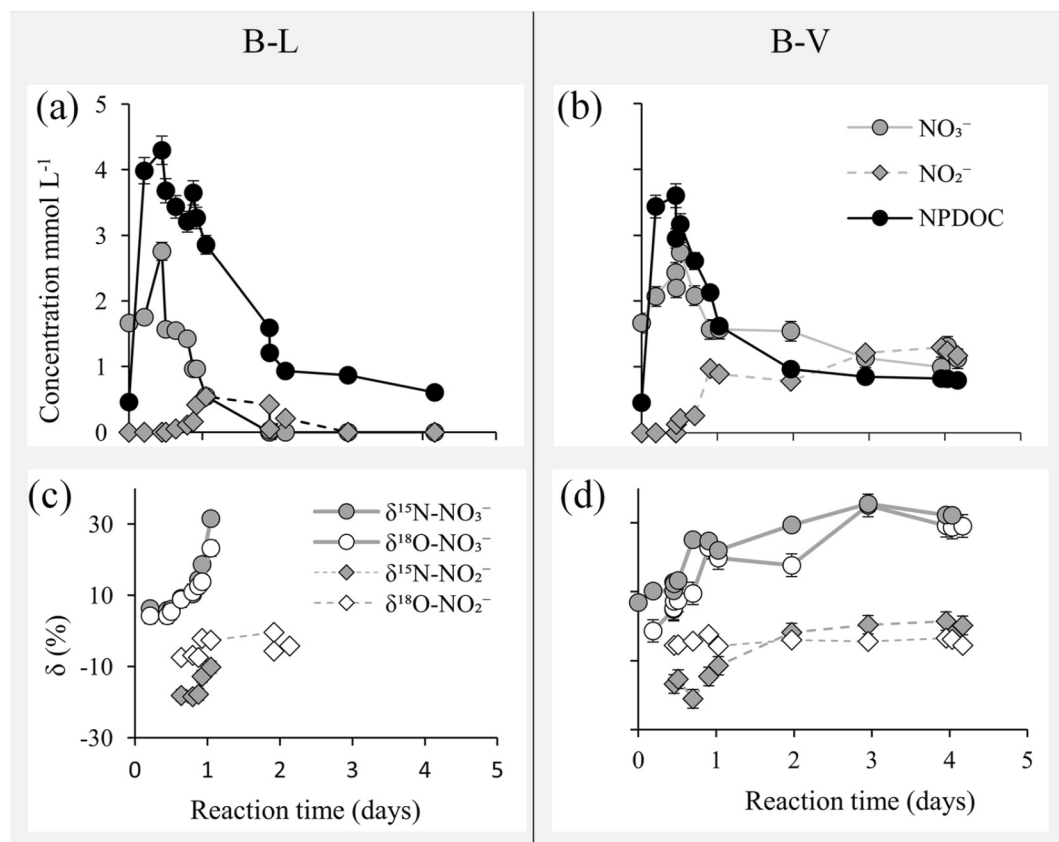


**Figure 3.** Chemical and isotopic results in B-L and B-V: evolution of  $\text{NO}_3^-$ ,  $\text{NO}_2^-$ , and NPDOC concentration in (a) B-L and (b) B-V experiments; evolution of  $\delta^{15}\text{N}$  and  $\delta^{18}\text{O}$  of  $\text{NO}_3^-$  and  $\text{NO}_2^-$  in (c) B-L and (d) B-V experiments. Error bars show a 5% error associated with experimental data; non-visible error bars are within the symbols.

associated with a significant  $\text{NO}_2^-$  accumulation during the entire experiment (up to 3 mM) (Figure 3b), attributed to the inhibition of  $\text{NO}_2^-$  reductase production due to incomplete  $\text{NO}_3^-$  attenuation (Kraft et al., 2011). This  $\text{NO}_2^-$  accumulation could be controlled by the organic carbon concentration, pH and bacterial community (Glass & Silverstein, 1998; Gómez et al., 2000). The pH identified in our batch experiments (7.6–7.9) was within the favorable pH range for  $\text{NO}_2^-$  reduction (Glass & Silverstein, 1998). Hence, bacterial growth was the main factor controlling  $\text{NO}_2^-$  accumulation; therefore, it could only be expected at the beginning of the treatment.

In batch experiments, NPDOC rapidly increased from 0.4 mM (NPDOC concentration field water) to peak concentrations of 4.3 mM in B-L and 3.6 mM in B-V after injecting the wine wastes. NPDOC concentration gradually decreased afterward to 0.6 mM in B-L and 0.8 mM in B-V (Figures 3a and 3b). The oxidation of organic matter increased bicarbonate concentration in the outflow water (from 4.8 to 7.2 mM in B-L and from 5.2 to 6.2 mM in B-V). High labile organic carbon in B-L suggests high organic carbon consumption, producing more bicarbonate, which explains the low residual NPDOC and high bicarbonate concentration observed in B-L (Table S2).

Geochemical calculations have shown that calcite was oversaturated in the outflow water ( $\text{SI} = 0.7$  in B-L and 0.6 in B-V) (Tables S2 and S3). The equilibrium with amorphous calcite may explain the buffering of pH in the batch experiments, keeping the pH constant over time. Calcite precipitation has also been observed in similar biological denitrification experiments (Mastroicco et al., 2011; Rodríguez-Escales et al., 2014).

Figures 3c and 3d show  $\delta^{15}\text{N}$  and  $\delta^{18}\text{O}$  of  $\text{NO}_3^-$  and  $\text{NO}_2^-$  versus time for B-L and B-V, respectively. During both experiments, the residual  $\text{NO}_3^-$  became enriched in the heavy isotopes over time, correlating with a decrease in  $\text{NO}_3^-$  concentration.  $\delta^{15}\text{N-NO}_3^-$  and  $\delta^{18}\text{O-NO}_3^-$  increased from +6.2‰ and +4.2‰ to +31.5‰ and +23.2‰, respectively in B-L (Figure 3c), and increased from -1.4‰ and +6.9‰ to +29.1‰ and +32.2‰ respectively in

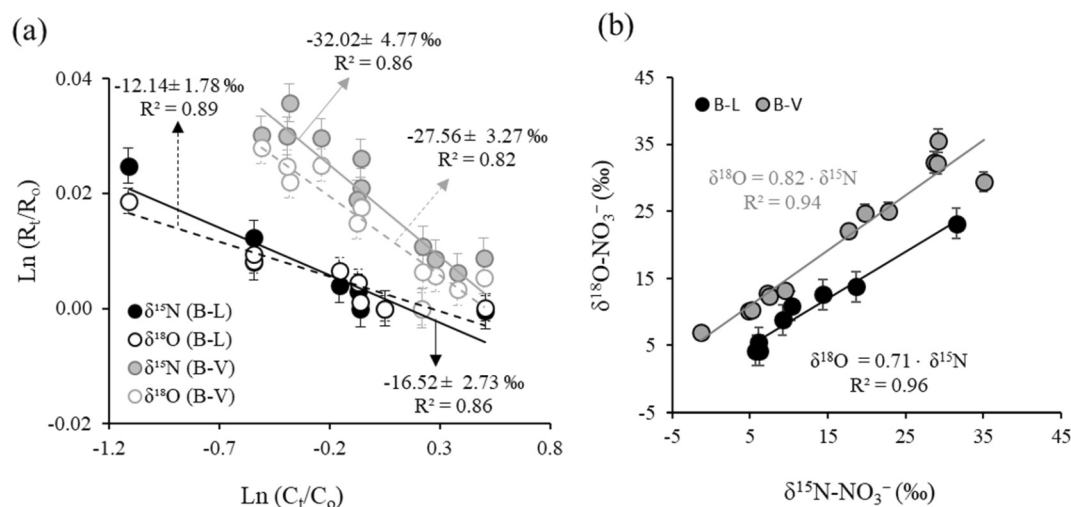


**Figure 4.** Isotopic data analyses in B-L and B-V: (a) evolution of the natural logarithm of the substrate remaining fraction ( $C_t/C_0$ ) versus the isotope ratios ( $R_t/R_0$ ) with slopes corresponding to the isotopic fractionation values in B-L and B-V. Solid continuous lines show the regression line for N with the slope indicated by the solid arrow lines, and dashed lines show the regression line for O with the slopes indicated by dashed arrow lines. (b) A plot of  $\delta^{15}\text{N}$  against  $\delta^{18}\text{O}$  showing a positive linear correlation in B-L and B-V and the regression line showing the slope ( $\epsilon/\epsilon\text{N}$ ). Error bars show a 5% error associated with experimental data; non-visible error bars are within the symbols.

B-V (Figure 3d). The enrichment of the heavy isotopes indicates that  $\text{NO}_3^-$  attenuation in these experiments was caused by denitrification (Carrey et al., 2013; Kendall et al., 2007). Because of the low C/N ratio in our study, we discarded the possibility of DNRA, which has been found to be important in high C and low  $\text{NO}_3^-$  conditions at C/N ratios greater than 5 (Burgin & Hamilton, 2007). The  $\text{NO}_2^-$  produced progressively became enriched in the heavy isotopes with  $\delta^{15}\text{N-NO}_2^-$  increasing from  $-18.5\text{‰}$  to  $-10.2\text{‰}$  in B-L (Figure 3c) and from  $-21.1\text{‰}$  to  $-1.5\text{‰}$  in B-V (Figure 3d). Since during denitrification, the  $\delta^{18}\text{O-NO}_2^-$  may equilibrate with  $\delta^{18}\text{O-H}_2\text{O}$  (Kool et al., 2007), a progressive increase of  $\delta^{18}\text{O-NO}_2^-$  was not observed in the batch experiments (Figures 3c and 3d). The natural logarithm of the remaining  $\text{NO}_3^-$  fraction ( $C_t/C_0$ ) was linearly correlated with the Ln of the isotope ratios ( $R_t/R_0$ ) with the slope representing  $\epsilon$ .  $\epsilon^{15}\text{N}_{\text{NO}_3}$  and  $\epsilon^{18}\text{O}_{\text{NO}_3}$  were  $-16.5 \pm 2.7\text{‰}$  and  $-12.1 \pm 1.8\text{‰}$  respectively in B-L, and  $-32.0 \pm 4.8\text{‰}$  and  $-27.6 \pm 3.3\text{‰}$  respectively in B-V (Figure 4a). The calculated  $\epsilon^{15}\text{N}_{\text{NO}_2}$  fractionation was  $-3.5 \pm 0.9\text{‰}$  ( $R^2 = 0.81$ ) and  $-7.8 \pm 2.2\text{‰}$  ( $R^2 = 0.62$ ) for B-L and B-V, respectively.

Limited  $\text{NO}_3^-$  removal in the case of B-V might show larger fractionation (i.e., more negative  $^{15}\epsilon$ ) values consistent with Mariotti et al. (1988), who proposed that larger fractionation is expected for a lower denitrification rate. The  $\epsilon^{15}\text{N}_{\text{NO}_3}$  and  $\epsilon^{18}\text{O}_{\text{NO}_3}$  obtained in our work are consistent with values reported in the literature for denitrification, ranging from  $+6.5$  to  $-39.0\text{‰}$  and  $-1.0$  to  $-30.4\text{‰}$ , respectively (Grau-Martínez et al., 2017; Margalef-Martí, Carrey, Merchán, et al., 2019) for freshwater denitrification studies, depending on the environmental conditions, organic matter source employed and biomass community.  $\delta^{15}\text{N-NO}_3^-$  versus  $\delta^{18}\text{O-NO}_3^-$  showed a positive linear correlation with a slope of 0.71 in B-L and 0.82 in B-V (Figure 4b), indicating a high enrichment effect on  $\epsilon^{15}\text{N}_{\text{NO}_3}$ . Although these values agree with literature ratios for biological denitrification (1–0.5), they are not consistent regarding many laboratory studies where the ratio is close to 1 (Carrey et al., 2014; Kendall et al., 2007). The deviation could be explained by  $\text{NO}_2^-$  reoxidation to  $\text{NO}_3^-$ , the type of bacteria involved in  $\text{NO}_3^-$  reduction or the reduction rate of  $\text{NO}_3^-$  (Buchwald & Casciotti, 2010; Casciotti, 2009; Granger & Wankel, 2016; Wunderlich et al., 2013).  $\epsilon^{18}\text{O}_{\text{NO}_3}/\epsilon^{15}\text{N}_{\text{NO}_3}$  ratio at the field scale can be influenced by atmospheric nitrate deposition, which can difficultate the denitrification influence on nitrate isotope composition assessment (Elliott et al., 2019). Denitrification has often been shown to exhibit a greater enrichment effect on  $\delta^{15}\text{N}_{\text{NO}_3}$  than  $\delta^{18}\text{O}_{\text{NO}_3}$ , which is seldom affected by denitrification in field-scale studies ( $\epsilon^{18}\text{O}_{\text{NO}_3}/\epsilon^{15}\text{N}_{\text{NO}_3}$  close to 0.5) (Critchley et al., 2014; Otero et al., 2009).  $\epsilon^{18}\text{O}_{\text{NO}_3}$  to  $\epsilon^{15}\text{N}_{\text{NO}_3}$  ratios serve as an indicator of denitrification efficiency and enable the distinction between bacterial activity and other processes that lead to a reduction in nitrate concentration without affecting the isotopic composition (Buyanjargal et al., 2023; Kendall et al., 2007). The batch degradation results have shown that *lilas* has the potential to remove  $\text{NO}_3^-$  from the water through



denitrification at a C/N ratio of 1.25, and  $\text{NO}_3^-$  attenuation is coupled with quick removal of  $\text{NO}_2^-$  from water. Under similar experimental conditions, *vinico* could only remove about 35% of  $\text{NO}_3^-$ , not enough to obtain  $\text{NO}_3^-$  concentrations below the required limit ( $0.81 \text{ mmol L}^{-1}$ ), and  $\text{NO}_2^-$  accumulated in water, exceeding the maximum concentration allowed ( $0.11 \text{ mM NO}_2^-$ ). Because of this different behavior, *lias* was chosen for the experimental column study, while *vinico* was discarded. The goal of the column experiment was to determine the efficacy of continuous treatment and to model the results for a better understanding of  $\text{NO}_3^-$  attenuation dynamics prior to a field upscaling.

### 3.2. Column Results and Discussion

The results of the column experiment with *lias* are summarized in Table S4. *Las* was injected daily into the column until day 4. During biostimulation, conductivity and pH averaged  $2.2 \pm 0.2 \text{ mS cm}^{-1}$  and  $8.2 \pm 0.1$ , respectively, with no significant fluctuations in time. Eh slightly increased from 0.19 to 0.23 V at the beginning of the experiment and decreased afterward to 0.14 V. Eh evolution demonstrated that the injection of *lias* created reducing conditions in the column, which were necessary for  $\text{NO}_3^-$  reduction.

Unlike the batch experiments, no initial increase in  $\text{NO}_3^-$  concentration was identified in the outflow water of the column experiment (Figure 4a); therefore,  $\text{NO}_3^-$  injected with *lias* was either not transported or consumed in the column.

$\text{NO}_3^-$  attenuation began quickly after the first injection, and  $\text{NO}_3^-$  was removed entirely from the outflow water in 3 days (Figure 5a).  $\text{NO}_3^-$  remained undetected in the outflow until day 7.  $\text{NO}_3^-$  recovery began after day seven and fully recovered to the initial concentration on day 10 (Figure 5a).  $\text{NO}_2^-$  did not significantly accumulate in the outflow water during the experiment. NPDOC concentration progressively increased from 0.4 mM to about 5.0 mM at the end of the injections (day 4–day 6). The increased NPDOC in the outflow water is attributed to external C supplied by *lias*. NPDOC quickly decreased to 0.8 mM on day seven (Figure 5a) and remained the same throughout the experiment. Similar to the results observed in the batch experiments, the  $\delta^{15}\text{N}$  and  $\delta^{18}\text{O}$  of  $\text{NO}_3^-$  increased over time (Figure 5b).  $\delta^{15}\text{N-NO}_3^-$  and  $\delta^{18}\text{O-NO}_3^-$  increased from +6.6 and +1.7‰ to +23.5 and +17.1‰, respectively (Figure 5b). Typical of denitrification, the natural logarithm of the substrate's remaining fraction was correlated to the isotope ratios by a negative linear relationship (Figure 5c). The calculated  $\epsilon^{15}\text{N}_{\text{NO}_3}$  and  $\epsilon^{18}\text{O}_{\text{NO}_3}$  were  $-17.7 \pm 2.9\%$  and  $-17.9 \pm 1.6\%$ , respectively (Figure 5c), and the  $\epsilon^{18}\text{O}_{\text{NO}_3}/\epsilon^{15}\text{N}_{\text{NO}_3}$  obtained in C-L is 1.0, characteristic of laboratory biological denitrification studies (Carrey et al., 2013; Grau-Martínez et al., 2017). Similar to B-L,  $\delta^{15}\text{N-NO}_3^-$  versus  $\delta^{18}\text{O-NO}_3^-$  bi-isotopic plot showed a positive linear correlation with a slope of 0.93 in C-L (Figure 5d), confirming denitrification as the  $\text{NO}_3^-$  attenuation pathway, as in the batch experiment. Similar to the batch experiments,  $\delta^{15}\text{N}$  of the generated  $\text{NO}_2^-$  increased from  $-3.4$  to  $+12.8\%$  and  $\delta^{18}\text{O-NO}_2^-$  equilibrated with  $\delta^{18}\text{O-H}_2\text{O}$ .

The isotopic data of the column experiment implies that any additional nitrate supplied by the wine waste underwent degradation within the column and did not reach the outflow reservoir. As a result, we did not observe the mixing of the heavy isotopes of the residual nitrate with fresh nitrate provided by the wine waste during the injection period. Consequently, the Rayleigh equation successfully reproduced the experimental data, treating it as a closed system. The similar  $\epsilon$  values observed in batch and column *lias* experiments suggest that the same processes were degrading  $\text{NO}_3^-$  in both experiments, attributed to the same organic matter source (*lias*) used. It also demonstrates that various factors such as nitrate supply, variations in biomass, mixing, flow velocity, and the potential presence of preferential flow paths in the column did not significantly impact the denitrification process within the column experiment. This conclusion is further supported by the fact that complete nitrate degradation was achieved in similar timeframes. The calculated laboratory isotope fractionation values are valuable for estimating denitrification efficiency for environmental applications. Laboratory-determined fractionation values are more reliable for quantifying denitrification efficiency than field fractionation values, as field values can overestimate denitrification rates (Böttcher et al., 1990; Mariotti et al., 1988). Therefore, controlled laboratory-scale fractionation values help to mitigate potential interferences from other attenuation processes under field conditions, establishing a more reliable basis for quantifying denitrification efficiency. However, applying these values to field-scale studies is challenging due to the natural variability influenced by factors like soil composition, microbial communities, and substrate availability (Maggi & Riley, 2009, 2010). Field-specific dynamics like transport and mixing (Green et al., 2010) and environmental changes such as temperature fluctuations, pH shifts and  $\text{O}_2$  levels (Druhan et al., 2014) make it challenging to apply laboratory-derived fractionation values to

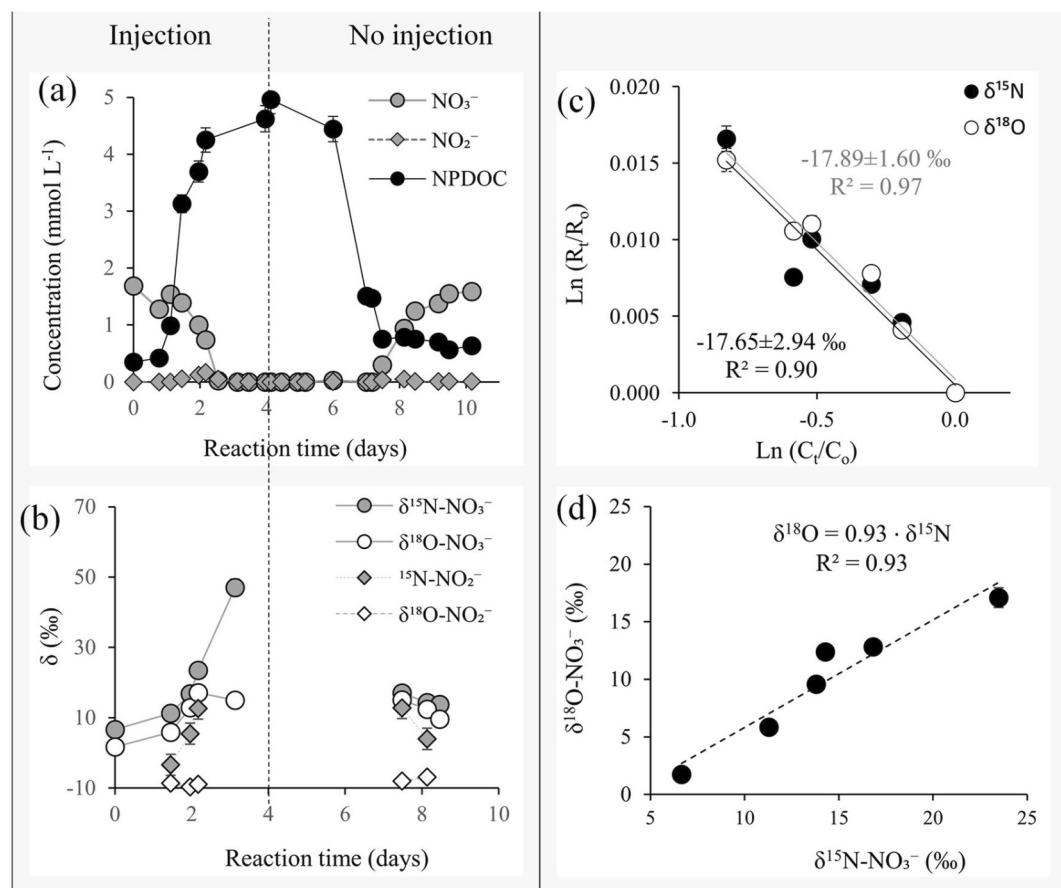


**Figure 5.** Chemical and isotopic data analyses: (a)  $\text{NO}_3^-$ ,  $\text{NO}_2^-$ , and NPDOC evolution in C-L. (b) Evolution of  $\delta^{15}\text{N}$  and  $\delta^{18}\text{O}$  of  $\text{NO}_3^-$  and  $\text{NO}_2^-$  over time in C-L. The dashed vertical line separates the injection period from the no-injection period (a and b). (c) A plot of the natural logarithm of the substrate remaining fraction against the isotope ratios showing a negative linear correlation with slopes depicting the isotopic fractionation values in C-L. (d) A plot  $\delta^{15}\text{N}$  against  $\delta^{18}\text{O}$  showing a positive linear correlation in C-L. Error bars show a 5% error associated with experimental data with non-visible error bars within the symbols.

field denitrification accurately. In order to ensure greater accuracy and precision in the laboratory findings and numerical models for field-scale applications, it is necessary to perform robust field measurements and establish long-term monitoring protocols to accommodate the intricate and constantly evolving dynamics of natural systems.

The batch and column experiments have shown that *lías* is a viable electron donor capable of inducing denitrification in nitrate-contaminated water. *Lías* does not seem to pose a pollution risk, as the concentration of heavy metals remained unchanged before and after the injection of *lías*, suggesting that *lías* does not contain heavy metal concentration high enough to significantly increase the levels in the field water, making it a safe option for remediating nitrate-polluted water bodies. According to the results obtained in this study, the electron donor feeding strategy is considered appropriate for future field application at the CW to improve denitrification efficiency.

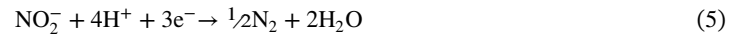
## 4. Geochemical Modeling

### 4.1. Conceptual Model

The model describes the coupled reaction between  $\text{NO}_3^-$  reduction and organic matter oxidation, linked to denitrifying bacterial growth and decay and the evolution of  $\text{NO}_3^-$  and  $\text{NO}_2^-$  isotopic composition in a fully

saturated system at a constant temperature of 25°C. The same conceptual model has been used to model the batch and column experiments.

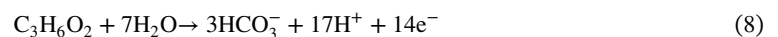
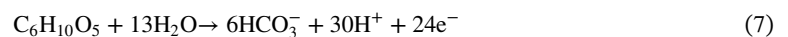
NO<sub>3</sub><sup>-</sup> reduction is assumed to occur in a two-step process. In the first step, nitrate is reduced to nitrite according to Reaction 4; in the second step, nitrite is reduced to dinitrogen gas according to Reaction 5.



Reactions 4 and 5 are assumed to be kinetically driven and are quantified using the dual Monod kinetics, the most used approach in biological denitrification models (Calderer et al., 2010; Chen & MacQuarrie, 2004). Monod kinetics assumes that the degradation rates are limited by both the electron donor and the electron acceptor concentration. In our model, Reactions 4 and 5 are quantified using Equation 6, where R<sub>EA</sub> is the NO<sub>3</sub><sup>-</sup> (for Reaction 4) or NO<sub>2</sub><sup>-</sup> (for Reaction 5) degradation rate (mol L<sup>-1</sup> s<sup>-1</sup>), [EA] is the electron acceptor concentration (NO<sub>3</sub><sup>-</sup> or NO<sub>2</sub><sup>-</sup> depending on the reaction) (mol L<sup>-1</sup>), [ED] is *lías/vínico* concentration (mol L<sup>-1</sup>), K<sub>EA</sub> and K<sub>ED</sub> are the electron acceptor and electron donor half-saturation constants respectively (mol L<sup>-1</sup>), k<sub>max</sub> is the maximum rate of the electron donor consumption (s<sup>-1</sup>), and [X<sub>EA</sub>] is biomass concentration (mol L<sup>-1</sup>), which is different for each Reactions 4 and 5. k<sub>max</sub> indicates the maximum rate at which the biological process can occur when substrate concentration is not limiting, while the half-saturation constants reflect the microorganism's affinity for a specific nutrient, representing the limiting nutrient concentration at which it can grow at half its maximum rate.

$$R_{EA} = -k_{\max} \cdot [X_{EA}] \cdot \left( \frac{[EA]}{[EA] + K_{EA}} \right) \cdot \left( \frac{[ED]}{[ED] + K_{ED}} \right) \quad (6)$$

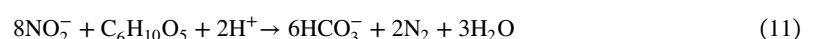
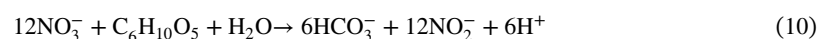
Reactions 4 and 5 are linked to the oxidation of *lías* and *vínico*. In our study, we did not conduct a specific analysis to determine the organic matter composition of the *lías* stimulant employed in our research. Previous investigations have extensively examined polysaccharides in the context of biological denitrification studies (Kim et al., 2002; Liu et al., 2013). Considering the observed fractionation values compared to existing literature, we infer that the labile organic carbon source contributing to the enhancement of denitrification in our study likely exhibits similarity with those previously characterized for polysaccharides. For the sake of simplicity, the simplest polysaccharide, C<sub>6</sub>H<sub>10</sub>O<sub>5</sub>, is considered representative of *lías*, and the simplest fatty acid, C<sub>3</sub>H<sub>5</sub>O<sub>2</sub>, is considered to represent *vínico*. The oxidation of these compounds occurs according to Reactions 7 and 8.

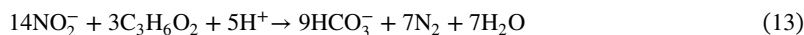
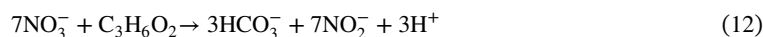


The rate of Reactions 7 and 8 is given by Equation 9, where k is the specific rate of organic matter degradation (dimensionless), [ED] is the concentration of C<sub>6</sub>H<sub>10</sub>O<sub>5</sub> for Reaction 7 or the concentration of C<sub>3</sub>H<sub>5</sub>O<sub>2</sub> for Reaction 8 (mol L<sup>-1</sup>), and R<sub>NO<sub>3</sub><sup>-</sup></sub> and R<sub>NO<sub>2</sub><sup>-</sup></sub> are the degradation rates of nitrate and nitrite, respectively, calculated with Equation 6.

$$R_{OM} = k \cdot [ED] \cdot [k_1 \cdot R_{\text{NO}_3^-} + k_2 \cdot R_{\text{NO}_2^-}] \quad (9)$$

k<sub>1</sub> and k<sub>2</sub> are the ratios of the stoichiometric coefficient between the organic carbon and the electron acceptor (C/N) in a balanced chemical reaction. In the case of *lías*, k<sub>1</sub> and k<sub>2</sub> were 0.5 and 0.75, respectively, according to Reactions 10 and 11. For *vínico*, k<sub>1</sub> and k<sub>2</sub> took values of 0.43 and 0.64, according to Reactions 12 and 13. k<sub>1</sub> and k<sub>2</sub> relate nitrate/nitrite reduction to organic matter consumption, which directly affects the rate and efficiency of denitrification processes.





The model considers that bacterial communities degrading nitrate and nitrite are different, as well as those degrading *lías* and *vínico*. The value of  $[\text{X}_{\text{EA}}]$  in Equation 6 will depend on each specific case (the organic matter used and the reduction step). The growth and decay of biomass concentration of each bacterial community ( $[\text{X}_{\text{EA}}]$ ,  $\text{mol L}^{-1} \text{ s}^{-1}$ ) are calculated according to Equation 14, where  $b$  and  $Y$  are the biomass decay constant and biomass growth yield coefficient, respectively (dimensionless and different for each bacterial community), and  $R_{\text{EA}}$  is the degradation rate of nitrate or nitrite, calculated according to Equation 6. The bacterial growth yield represents the amount of biomass generated for each unit of organic matter consumed, while the decay constant indicates the rate at which bacteria die in the absence of sufficient organic matter.

$$R_{\text{X}_{\text{EA}}} = -Y \cdot R_{\text{EA}} - b \cdot [\text{X}_{\text{EA}}] \quad (14)$$

The change in the isotopic composition of N in nitrate and nitrite ( $\delta^{15}\text{N-NO}_3^-$  and  $\delta^{15}\text{N-NO}_2^-$ ) during denitrification has been modeled according to the first-order degradation kinetics described in Van Breukelen and Prommer (2008) and shown in Equation 15, where  $\epsilon$  is the isotope fractionation (i.e., different for nitrate and nitrite),  $[\delta^{\text{H}}\text{EA}]/([\delta^{\text{H}}\text{EA}] + [\delta^{\text{L}}\text{EA}])$  is N isotope ratio of  $\text{NO}_3^-$  and  $\text{NO}_2^-$ , and  $R_{\text{EA}}$  is the degradation rate of nitrate or nitrite, calculated from Equation 6.

$$R_{\delta^{\text{H}}\text{EA}} = R_{\text{EA}} \cdot \frac{[\delta^{\text{H}}\text{EA}]}{[\delta^{\text{H}}\text{EA}] + [\delta^{\text{L}}\text{EA}]} \cdot \epsilon \quad (15)$$

Aqueous speciation is assumed to occur in equilibrium, and concentrations are calculated with the mass action law, which has been considered for all the aqueous species listed in Table S5 of the Supporting Information S1. To be consistent with the experimental data, a constant  $\text{CO}_2$  partial pressure of  $10^{-2.6}$  atm has been considered, and calcite precipitation in equilibrium is allowed, following the principles of the mass action law using the iso.dat database. Instead of using amorphous calcite, for which thermodynamic data was unavailable in the database, crystalline calcite has been used but is only left to precipitate for saturation indices higher than 0.7.

A homogeneous porous substrate media is considered for the batch reactions and transport models. The column transport model has considered one-dimensional transport due to advection and diffusion coupled with chemical reactions under a constant flow.

## 4.2. Numerical Model

The initial pore water composition for the batch and column models is the field water composition (FW) in Table S2. An initial nitrate concentration of 2.8 mM with initial  $\delta^{15}\text{N-NO}_3^- = +5.7\text{‰}$  and  $\delta^{18}\text{O-NO}_3^- = +4.3\text{‰}$  for B-L and 2.6 mM with initial  $\delta^{15}\text{N-NO}_3^- = +4.8\text{‰}$  and  $\delta^{18}\text{O-NO}_3^- = +10.3\text{‰}$  for B-V were considered for the batch models after peak nitrate increase due the wine waste injection and dissolution in 12 hr. In the C-L, nitrate measurements at the top of the column did not reveal a concentration rise from wine waste injection and an initial nitrate concentration of 1.7 mM with initial  $\delta^{15}\text{N-NO}_3^- = +6.6\text{‰}$  and  $\delta^{18}\text{O-NO}_3^- = +1.7\text{‰}$  was chosen. In both the batch and column models,  $\text{NO}_2^-$  and  $\text{N}_2$  initial concentrations were set at 0  $\text{mmol L}^{-1}$ . After some preliminary calculations, an initial biomass concentration of 0.005  $\text{mol L}^{-1}$  and 0.003  $\text{mol L}^{-1}$  were chosen for the *lías* and *vínico* experiments, respectively, and an initial concentration of organic matter of 0.4 mM obtained from the experimental results was chosen in both cases. In our models, the average isotopic fractionation values based on our experimental results,  $\epsilon^{15}\text{N}_{\text{NO}_3} = -18\text{‰}$  and  $\epsilon^{15}\text{N}_{\text{NO}_2} = -4\text{‰}$  for B-L/C-L and  $\epsilon^{15}\text{N}_{\text{NO}_3} = -29\text{‰}$  for B-V, have been chosen for Equation 15. The initial moles of calcite were set to zero in phase assemblage, allowing calcite to precipitate at saturation indices  $>0.7$ . The values of the reaction rate parameters ( $k_{\text{max}}$ ,  $K_{\text{ED}}$ ,  $K_{\text{EA}}$ ,  $Y$ ,  $k$ , and  $b$ ) for Equations 2–4 were initially those from Rodríguez-Escalles et al. (2014), who conducted batch experiments under similar experimental conditions (Table 1).

The column experiment was modeled considering a one-dimensional system of 70 cm length discretized in 70 cells of 1 cm length. A constant temperature of 25°C was chosen in the batch and transport simulations. No

**Table 1**  
*Numerical Model Parameters*

Model parameter	Range of values	Initial guess	Fitted values	
			B-L/C-L	B-V
$K_{EA,NO_3^-}$ (mol L <sup>-1</sup> )	$1.0 \times 10^{-6}$ – $1.7 \times 10^{-4}$ <sup>a,b,c,d,e</sup>	$1.4 \times 10^{-5}$	$5.0 \times 10^{-4}$	$5.0 \times 10^{-4}$
$K_{EA,NO_2^-}$ (mol L <sup>-1</sup> )	$1.0 \times 10^{-6}$ – $1.7 \times 10^{-4}$ <sup>a,b,c,d,e</sup>	$1.4 \times 10^{-5}$	$6.0 \times 10^{-5}$	$6.0 \times 10^{-5}$
$K_{ED,NO_3^-}$ (mol L <sup>-1</sup> )	$8.3 \times 10^{-6}$ – $1.0 \times 10^{-1}$ <sup>a,b,c,d,e</sup>	$2.2 \times 10^{-5}$	$2.2 \times 10^{-5}$	$2.2 \times 10^{-5}$
$K_{ED,NO_2^-}$ (mol L <sup>-1</sup> )	$8.3 \times 10^{-6}$ – $1.0 \times 10^{-1}$ <sup>a,b,c,d,e</sup>	$2.2 \times 10^{-5}$	$1.0 \times 10^{-6}$	$1.0 \times 10^{-6}$
$k_{max,NO_3^-}$ (s <sup>-1</sup> )	$1.0 \times 10^{-3}$ – $3.9 \times 10^{-7}$ <sup>a,b,c,d,e</sup>	$3.9 \times 10^{-7}$	$5.0 \times 10^{-7}$	$5.0 \times 10^{-7}$
$k_{max,NO_2^-}$ (s <sup>-1</sup> )	$5.2 \times 10^{-4}$ – $7.0 \times 10^{-8}$ <sup>a,b,c,d,e</sup>	$4.4 \times 10^{-7}$	$5.0 \times 10^{-7}$	$5.0 \times 10^{-7}$
Y,NO <sub>3</sub> <sup>-</sup> (moles C-cells/mol C-OC)	0.05–0.73 <sup>a,b,c,d,e,f</sup>	0.57	0.53	0.53
Y,NO <sub>2</sub> <sup>-</sup> (moles C-cells/mol C-OC)	0.05–0.73 <sup>a,b,c,d,e,f</sup>	0.57	0.53	0.53
b,NO <sub>3</sub> <sup>-</sup> (s <sup>-1</sup> )	$0$ – $5.8 \times 10^{-7}$ <sup>a,b,c,d,e</sup>	$1.2 \times 10^{-7}$	$3.0 \times 10^{-6}$	$3.2 \times 10^{-5}$
b,NO <sub>2</sub> <sup>-</sup> (s <sup>-1</sup> )	$0$ – $5.8 \times 10^{-7}$ <sup>a,b,c,d,e</sup>	$1.2 \times 10^{-7}$	$3.0 \times 10^{-6}$	$5.0 \times 10^{-5}$
k		210	950	1,400

*Note.* Fitted Reaction Rate Parameters for Equations Used in our Model Estimated From GibbsStudio (Batch and Column Experiments) and Reported Values in the Literature. <sup>a</sup>Chen and MacQuarrie (2004). <sup>b</sup>Killingstad et al. (2002). <sup>c</sup>Kinzelbach et al. (1991). <sup>d</sup>Mastrocicco et al. (2011). <sup>e</sup>Rodríguez-Escales et al. (2014). <sup>f</sup>Parkhurst and Appelo (2013).

flow and transport boundary conditions were considered for the batch models. However, for the column model, we employed forward flow and flux boundary conditions for the first and last cells. A velocity of  $3.5 \times 10^{-6}$  m s<sup>-1</sup>, a dispersivity of 0.005 m and a diffusion coefficient of  $3.0 \times 10^{-10}$  m<sup>2</sup> s<sup>-1</sup>, estimated from a conservative tracer test (Figure S1 and Table S6 of the Supporting Information S1), were used in the transport modeling.

The batch experiments models were run for four and a half days in 415 time steps, while the column model was run for 10 days in 2857 time steps. To ensure the numerical stability of the column model, the grid spacing and the step length fulfilled the Péclet number (<2) and the Courant number (<1).

### 4.3. Modeling Results

The initially estimated reaction rate parameters were calibrated using nitrate/nitrite concentration of our batch experiments with CeresStudy in GibbsStudio (Nardi & de Vries, 2017) to obtain the best fit. For comparison purposes, Table 1 presents our initial guesses, the range of values reported in the existing literature, and the best-fit parameters obtained through our calibration process. The associated uncertainties, calculated as the root mean square errors resulting from the Levenberg–Marquardt fitting algorithm, are detailed in Table S7 of the Supporting Information S1.

The batch model does not consider the increase of NO<sub>3</sub><sup>-</sup> concentration due to the dissolution of wine waste, and the initial time corresponds to the maximum NO<sub>3</sub><sup>-</sup> concentration reached in 12 hr. The simulated pH well reproduced the experimental results in both the batch and column experiments (Figure S2 of the Supporting Information S1). Eh quickly reduced from +0.28 to -0.19 V in B-L and B-V models and remained constant throughout the simulation.

In addition to nitrate, nitrite, dissolved organic carbon and biomass concentrations that several authors have modeled in biological denitrification (André et al., 2011; Green et al., 1995), our model incorporates nitrogen isotope composition of nitrate and nitrite, which has not gained much attention to a significant extent. Our model simulates the evolution of NO<sub>3</sub><sup>-</sup>, NO<sub>2</sub><sup>-</sup>, δ<sup>15</sup>N-NO<sub>3</sub><sup>-</sup> and δ<sup>15</sup>N-NO<sub>2</sub><sup>-</sup> in B-L and B-V (Figures 6a and 6c, respectively). The model also reproduces NPDOC concentration in B-L and B-V, shown in Figures 6b and 6d, respectively. Table S7 in Supporting Information S1 reveals a remarkably high level of accuracy achieved by your predictive model.



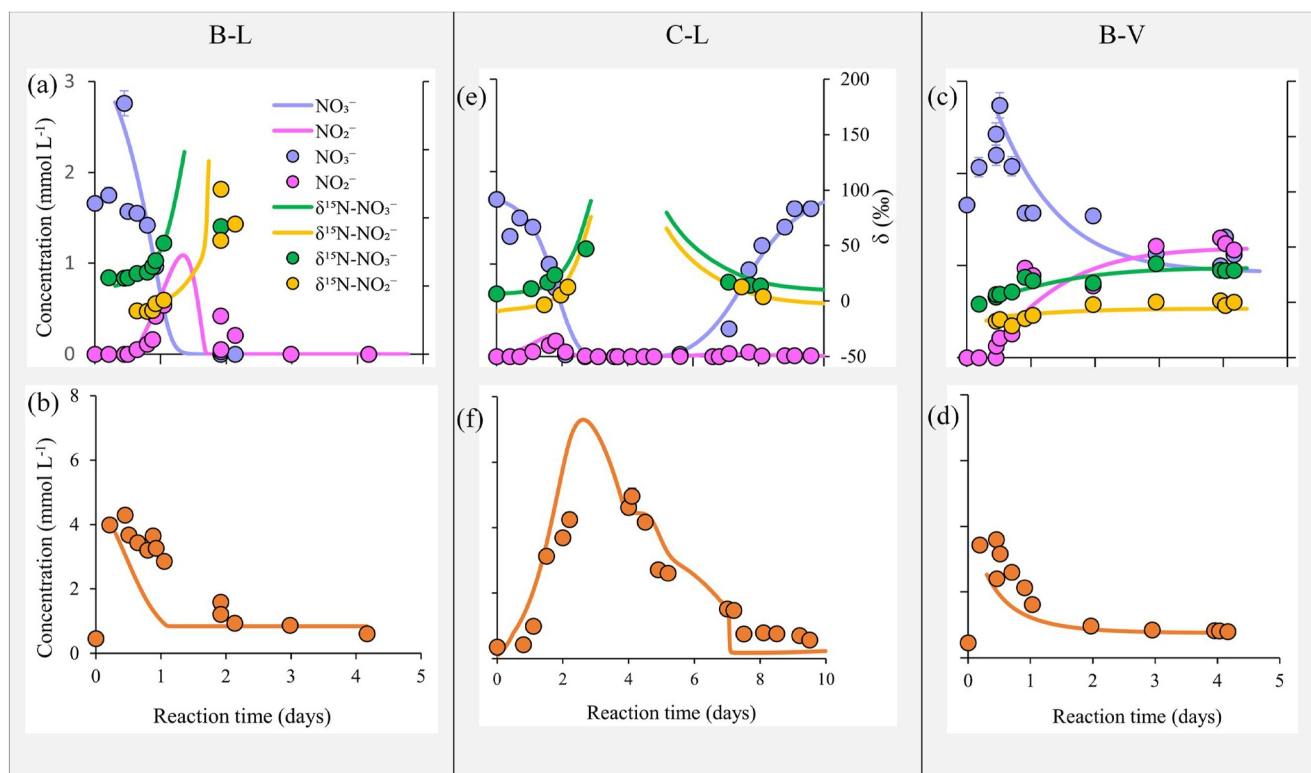


**Figure 6.** Modeling results (lines) versus experimental data (dots) for  $\text{NO}_3^-$ ,  $\text{NO}_2^-$ , and NPDOC concentrations and  $\delta^{15}\text{N}$  of  $\text{NO}_3^-$  and  $\text{NO}_2^-$  of the batch and column experiments. Error bars indicate a 5% margin of error with experimental data (non-visible error bars within circles).

Similarly to the experimental results,  $\text{NO}_3^-$  and  $\text{NO}_2^-$  were quickly removed from the solution in B-L, while in B-V,  $\text{NO}_3^-$  was not completely removed and was coupled to a high  $\text{NO}_2^-$  accumulation (Figures 6a and 6c).  $\text{NO}_3^-$  reduction in the model was related to the increase of  $\delta^{15}\text{N}\text{-NO}_3^-$  in the remaining  $\text{NO}_3^-$  fraction and the generated  $\text{NO}_2^-$ . An advantage of the geochemical isotope model is its ability to simulate  $\delta^{15}\text{N}$  of  $\text{NO}_3^-$  and  $\text{NO}_2^-$  at low  $\text{NO}_3^-$  and  $\text{NO}_2^-$  concentrations below the detection limit by laboratory measurements ( $0.2 \text{ mg L}^{-1}$  for  $\text{NO}_3^-$  and  $0.01 \text{ mg L}^{-1}$  for  $\text{NO}_2^-$ ). However, extremely low levels of  $\text{NO}_3^-$  and  $\text{NO}_2^-$  can result in very high isotopic values. When simulating  $\delta^{15}\text{N}\text{-NO}_2^-$  of the low  $\text{NO}_2^-$  experiment (B-L), the model fitted the experimental  $\delta^{15}\text{N}\text{-NO}_2^-$  using the experimentally determined  $\epsilon^{15}\text{N}_{\text{NO}_2}$  equal to  $-4\text{‰}$  but a higher  $\epsilon^{15}\text{N}_{\text{NO}_2}$  of  $-18\text{‰}$  instead of  $-8\text{‰}$  was imposed in B-V to accurately reproduce the experimental results. Similar  $\delta^{15}\text{N}\text{-NO}_2^-$  results were obtained by Sebilo et al. (2019) for a high  $\text{NO}_2^-$  system, where the model could simulate the experimental results by using a higher  $\epsilon^{15}\text{N}_{\text{NO}_2}$  of  $-10\text{‰}$  than the value obtained in batch experiments ( $-4.2\text{‰}$ ). The behavior of  $\epsilon^{15}\text{N}_{\text{NO}_2}$  in our models within a high-nitrite system may be associated with nitrite's potential reoxidation to nitrate, which was not previously considered. This is a crucial factor that should be incorporated into future models in the transferability of the laboratory results to field-scale studies.

By applying the same reaction rate parameters utilized in the B-L model, the C-L model demonstrates the capability to replicate the concentrations of  $\text{NO}_3^-$ ,  $\text{NO}_2^-$  and NPDOC, as well as  $\delta^{15}\text{N}$  of  $\text{NO}_3^-$  and  $\text{NO}_2^-$  accurately (Figures 5c and 5f). Because the peak  $\text{NO}_3^-$  concentration occurs at the start of the column experiment, the initial time of the column model coincides with the initial time of the experiment. Eh in the C-L model showed more pronounced reducing conditions up to day 4 ( $-0.26 \text{ V}$ ), probably due to the injection of *lías* in the column. Subsequently, Eh rapidly increased to  $0.75 \text{ V}$  and remained constant through day 10. Like the B-L model, the C-L model achieves complete removal of nitrogen species from the solution and simulates  $\delta^{15}\text{N}$  of  $\text{NO}_3^-$  and  $\text{NO}_2^-$  at low nitrate and nitrite concentrations (Figures 6c and 6f).

The same reaction rate parameters ( $k_{\text{max}}$ ,  $K_{\text{ED}}$ ,  $K_{\text{EA}}$ ,  $Y$ ,  $k$  and  $b$ ) used in B-L and C-L might have contributed to the slight discrepancy between experimental and model results, particularly NPDOC (Figures 6b and 6d). Our model assumed constant transport parameters throughout the column and over time. Most biomass often colonizes

around the injection point, thus, modifying the dispersivity and other associated transport parameters in the column, which has been reported in similar experiments (Kildsgaard & Engesgaard, 2001; Rodríguez-Escales et al., 2016). Other studies have shown that the biofilm colonization and calcite precipitation over time in biological remediation studies lasting more than 2 weeks tends to modify the porosity and hydraulic conductivity (Armon et al., 2005; Hill & Sleep, 2002; Seifert & Engesgaard, 2007).

The biomass dynamics suggest that endogenous respiration did not play a significant role in denitrification in our model. At complete  $\text{NO}_3^-$  exhaustion with no external carbon source, the biomass population remained steady with no substantial decay to provide additional carbon, which may explain the slight delay before the onset of  $\text{NO}_3^-$  recovery. Rodríguez-Escales et al. (2014), in batch experiments using glucose and ethanol as electron donors, found that endogenous respiration did not contribute significantly to nitrate reduction (less than 10%).

## 5. Conclusions

This work evaluates the denitrification potential of two industrial wine residues (*lías* and *vínico*), accomplished by characterizing batch and column experiments and using chemical and isotopic techniques. The efficiency of nitrate removal depended on the type of wine residue used. The batch results showed that *lías* had the capacity to promote complete nitrate attenuation at a C/N ratio of 1.25 with no hazardous intermediate products. Under similar experimental conditions, *vínico* could only attenuate 35% nitrate and was linked to a high  $\text{NO}_2^-$  accumulation. *Lías* was selected for the column experiment due to its high nitrate removal capacity. At the same C/N ratio, complete denitrification was achieved when *lías* was injected daily into the column for 4 days. The column experimental results indicate the viability of the controlled injection for utilizing wine waste in wetland applications to enhance denitrification rates during specific time intervals when denitrification processes are most active. The controlled injection method offers flexibility in adjusting injection parameters to achieve high denitrification rates. However, it emphasizes the importance of tailoring wine waste application to the characteristics and limitations of the specific wetland site.

The calculated isotope fractionation ( $\epsilon^{15}\text{N}_{\text{NO}_3}$  and  $\epsilon^{18}\text{O}_{\text{NO}_3}$ ) in the batch experiments with *vínico* were  $-32 \pm 5\%$  and  $-28 \pm 3\%$ , respectively, while with *lías*,  $\epsilon^{15}\text{N}_{\text{NO}_3}$  and  $\epsilon^{18}\text{O}_{\text{NO}_3}$  were  $-17 \pm 3\%$  and  $-12 \pm 2\%$ , respectively, in batch experiments and  $-18 \pm 3\%$  and  $-18 \pm 2\%$ , respectively, in column experiments. Laboratory-derived isotope fractionation values are valuable for quantifying denitrification efficiency in environmental applications, providing greater reliability than field-based values. However, applying these laboratory values to field-scale studies is challenging due to natural variability and environmental dynamics. Robust field measurements and long-term monitoring protocols are essential to ensure more accurate results in applying controlled laboratory results in numerical models and field settings.

The developed numerical model described the transformation of nitrogen species in the batch and column experiments by combining nitrate and nitrite respiration, nitrate and nitrite reducing bacterial growth and decay, organic matter oxidation, calcite precipitation reactions and nitrate and nitrite isotopic fractionation. Using experimental and model data allows a comprehensive understanding of the processes occurring during nitrate attenuation and could be useful in field studies.

## Data Availability Statement

Supporting Information S1 and the experimental data used in this study are freely available on Zenodo (Abu et al., 2023). The Phreeqc version three software used in this work is available online at <https://water.usgs.gov/water-resources/software/PHREEQC/index.html>, and the GibbsStudio version three software is also available at <https://gibbsstudio.io/>.

## References

- Abraham, R., Causapé, J., Moreno-Mateos, D., & Comín, F. (2013). Nitrate and salt water contamination associated with the transition of an agrarian basin into an irrigated area. *Water Environment Research*, 85(2), 105–112. <https://doi.org/10.2175/106143012x13560205144254>
- Abu, A., Carrey, R., Navarro-Ciurana, D., Margalef-Martí, R., Albert, S., Neus, O., & Domènech, C. (2023). Chemical and isotopic data of laboratory batch and column experiments using industrial wine wastes to biostimulate denitrification [Dataset]. *Zenodo*. <https://doi.org/10.5281/zenodo.8027789>
- Abu, A., Carrey, R., Valhondo, C., Domènech, C., Otero, N., Soler, A., et al. (2022). Pathways and efficiency of nitrogen attenuation in wastewater effluent through soil aquifer treatment. *Journal of Environmental Management*, 321. <https://doi.org/10.2139/ssrn.4127243>

### Acknowledgments

This publication is part of the Grant PACE-ISOTEC (CGL2017-87216-C4-1-R) funded by MICIU/AEI/10.13039/501100011033 and by “ERDF A way of making Europe,” the Grant REMEDIATE (TED2021-131005B-C31) funded by MICIU/AEI/10.13039/501100011033 and by “European Union NextGenerationEU/PRTR,” the Grant NPP-SOL (PCI2023-143359) funded by MICIU/AEI/10.13039/501100011033 and co-funded by the European Union under the “PRIMA2022 Programme-Section2” and the project AgroSOS (PID2019-108057RB-I00) funded by MICIU/AEI/10.13039/501100011033 and by “ERDF/EU”. It has also been funded by Generalitat de Catalunya through the Consolidated Research Group MAGH (2021-SGR-00308). The authors are thankful to the CCiT of the Universitat de Barcelona for the analytical support. Abu Alex would also like to thank the Agency for Management of University and Research Grants of the Generalitat de Catalunya and Fundació Bosch i Gimpera de la Universitat de Barcelona for the PhD Grant (2019\_FL\_B 01059) and the L’Institut de Recerca de l’Aigua (IdRA)-Universitat de Barcelona for their support. We are grateful to the reviewers for improving the quality of this paper.

- Akunna, J. C., Bizeau, C., & Moletta, R. (1993). Nitrate and nitrite reductions with anaerobic sludge using various carbon sources: Glucose, glycerol, acetic acid, lactic acid and methanol. *Water Research*, 27(8), 1303–1312. [https://doi.org/10.1016/0043-1354\(93\)90217-6](https://doi.org/10.1016/0043-1354(93)90217-6)
- André, L., Pauwels, H., Dictor, M. C., Parmentier, M., & Azaroual, M. (2011). Experiments and numerical modelling of microbially-catalyzed denitrification reactions. *Chemical Geology*, 287(3–4), 171–181. <https://doi.org/10.1016/j.chemgeo.2011.06.008>
- Arnon, S., Adar, E., Ronen, Z., Yakirevich, A., & Nativ, R. (2005). Impact of microbial activity on the hydraulic properties of fractured chalk. *Journal of Contaminant Hydrology*, 76(3–4), 315–336. <https://doi.org/10.1016/j.jconhyd.2004.11.004>
- Beauchamp, E. G., Trevors, J. T., & Paul, J. W. (1989). Carbon sources for bacterial denitrification. *Advances in Soil Science*, 10, 113–142. [https://doi.org/10.1007/978-1-4613-8847-0\\_3](https://doi.org/10.1007/978-1-4613-8847-0_3)
- Böttcher, J., Strebel, O., Voerkelius, S., & Schmidt, H. L. (1990). Using isotope fractionation of nitrate-nitrogen and nitrate-oxygen for evaluation of microbial denitrification in a sandy aquifer. *Journal of Hydrology*, 114(3–4), 413–424. [https://doi.org/10.1016/0022-1694\(90\)90068-9](https://doi.org/10.1016/0022-1694(90)90068-9)
- Buchwald, C., & Casciotti, K. L. (2010). Oxygen isotopic fractionation and exchange during bacterial nitrite oxidation. *Limnology & Oceanography*, 55(3), 1064–1074. <https://doi.org/10.4319/lo.2010.55.3.1064>
- Burgin, A. J., & Hamilton, S. K. (2007). Have we overemphasized the role of denitrification in aquatic ecosystems? A review of nitrate removal pathways. *Frontiers in Ecology and the Environment*, 5(2), 89–96. [https://doi.org/10.1890/1540-9295\(2007\)5\[89:HWOTRO\]2.0.CO;2](https://doi.org/10.1890/1540-9295(2007)5[89:HWOTRO]2.0.CO;2)
- Buyanjargal, A., Kang, J., Lee, J. H., & Jeon, S. W. (2023). Nitrate removal rates, isotopic fractionation, and denitrifying bacteria in a woodchip-based permeable reactive barrier system: A long-term column experiment. *Environmental Science and Pollution Research*, 30(13), 36364–36376. <https://doi.org/10.1007/s11356-022-24826-4>
- Calderer, M., Gibert, O., Martí, V., Rovira, M., De Pablo, J., Jordana, S., et al. (2010). Denitrification in presence of acetate and glucose for bioremediation of nitrate-contaminated groundwater. *Environmental Technology*, 31(7), 799–814. <https://doi.org/10.1080/09593331003667741>
- Carrey, R., Otero, N., Soler, A., Gómez-Alday, J. J., & Ayora, C. (2013). The role of Lower Cretaceous sediments in groundwater nitrate attenuation in central Spain: Column experiments. *Applied Geochemistry*, 32, 142–152. <https://doi.org/10.1016/j.apgeochem.2012.10.009>
- Carrey, R., Otero, N., Vidal-Gavilan, G., Ayora, C., Soler, A., & Gómez-Alday, J. J. (2014). Induced nitrate attenuation by glucose in groundwater: Flow-through experiment. *Chemical Geology*, 370(2), 19–28. <https://doi.org/10.1016/j.chemgeo.2014.01.016>
- Casciotti, K. L. (2009). Inverse kinetic isotope fractionation during bacterial nitrite oxidation. *Geochimica et Cosmochimica Acta*, 73(7), 2061–2076. <https://doi.org/10.1016/j.gca.2008.12.022>
- Chen, D. J. Z., & MacQuarrie, K. T. B. (2004). Numerical simulation of organic carbon, nitrate, and nitrogen isotope behavior during denitrification in a riparian zone. *Journal of Hydrology*, 293(1–4), 235–254. <https://doi.org/10.1016/j.jhydrol.2004.02.002>
- Coplen, T. B. (2011). Guidelines and recommended terms for expression of stable-isotope-ratio and gas-ratio measurement results. *Rapid Communications in Mass Spectrometry*, 25(17), 2538–2560. <https://doi.org/10.1002/rcm.5129>
- Critchley, K., Rudolph, D. L., Devlin, J. F., & Schillig, P. C. (2014). Stimulating in situ denitrification in an aerobic, highly permeable municipal drinking water aquifer. *Journal of Contaminant Hydrology*, 171, 66–80. <https://doi.org/10.1016/j.jconhyd.2014.10.008>
- Druhan, J. L., Steefel, C. I., Conrad, M. E., & DePaolo, D. J. (2014). A large column analog experiment of stable isotope variations during reactive transport: I. A comprehensive model of sulfur cycling and  $\delta^{34}\text{S}$  fractionation. *Geochimica et Cosmochimica Acta*, 124, 366–393. <https://doi.org/10.1016/j.gca.2013.08.037>
- Elliott, E. M., Yu, Z., Cole, A. S., & Coughlin, J. G. (2019). Isotopic advances in understanding reactive nitrogen deposition and atmospheric processing. *Science of the Total Environment*, 662, 393–403. <https://doi.org/10.1016/j.scitotenv.2018.12.177>
- Glass, C., & Silverstein, J. (1998). Denitrification kinetics of high nitrate concentration water. *Water Research*, 32(3), 831–839. [https://doi.org/10.1016/S0043-1354\(97\)00260-1](https://doi.org/10.1016/S0043-1354(97)00260-1)
- Gómez, M. A., González-López, J., & Hontoria-García, E. (2000). Influence of carbon source on nitrate removal of contaminated groundwater in a denitrifying submerged filter. *Journal of Hazardous Materials*, 80(1–3), 69–80. [https://doi.org/10.1016/S0304-3894\(00\)00282-X](https://doi.org/10.1016/S0304-3894(00)00282-X)
- Granger, J., & Wankel, S. D. (2016). Isotopic overprinting of nitrification on denitrification as a ubiquitous and unifying feature of environmental nitrogen cycling. *Proceedings of the National Academy of Sciences of the United States of America*, 113(42), E6391–E6400. <https://doi.org/10.1073/pnas.1601383113>
- Grau-Martínez, A., Torrentó, C., Carrey, R., Rodríguez-Escapes, P., Domènech, C., Ghiglieri, G., & Otero, N. (2017). Feasibility of two low-cost organic substrates for inducing denitrification in artificial recharge ponds: Batch and flow-through experiments. *Journal of Contaminant Hydrology*, 198(2), 48–58. <https://doi.org/10.1016/j.jconhyd.2017.01.001>
- Green, C. T., Böhlke, J. K., Bekins, B. A., & Phillips, S. P. (2010). Mixing effects on apparent reaction rates and isotope fractionation during denitrification in a heterogeneous aquifer. *Water Resources Research*, 46(8), W08525. <https://doi.org/10.1029/2009WR008903>
- Green, M., Schnitzer, M., & Tarre, S. (1995). Kinetics of a fluidized-bed reactor for groundwater denitrification. *Applied Microbiology and Biotechnology*, 43(1), 188–193. <https://doi.org/10.1007/BF00170642>
- Hill, D. D., & Sleep, B. E. (2002). Effects of biofilm growth on flow and transport through a glass parallel plate fracture. *Journal of Contaminant Hydrology*, 56(3–4), 227–246. [https://doi.org/10.1016/s0169-7722\(01\)00210-8](https://doi.org/10.1016/s0169-7722(01)00210-8)
- Ioannou, L. A., Puma, G. L., & Fatta-Kassinos, D. (2015). Treatment of winery wastewater by physicochemical, biological and advanced processes: A review. *Journal of Hazardous Materials*, 286, 343–368. <https://doi.org/10.1016/j.jhazmat.2014.12.043>
- Kendall, C., Elliott, E. M., & Wankel, S. D. (2007). Tracing anthropogenic inputs of nitrogen to ecosystems. In *Stable isotopes in ecology and environmental science* (2nd ed., pp. 375–449).
- Kildsgaard, J., & Engesgaard, P. (2001). Numerical analysis of biological clogging in two-dimensional sandbox experiments. *Journal of Contaminant Hydrology*, 50(3–4), 261–285. [https://doi.org/10.1016/S0169-7722\(01\)00109-7](https://doi.org/10.1016/S0169-7722(01)00109-7)
- Killingstad, M. W., Widdowson, M. A., & Smith, R. L. (2002). Modeling enhanced in situ denitrification in groundwater. *Journal of Environmental Engineering*, 128(6), 491–504. [https://doi.org/10.1061/\(asce\)0733-9372\(2002\)128:6\(491\)](https://doi.org/10.1061/(asce)0733-9372(2002)128:6(491))
- Kim, Y. S., Nakano, K., Lee, T. J., Kanchanatawee, S., & Matsumura, M. (2002). On-site nitrate removal of groundwater by an immobilized psychrophilic denitrifier using soluble starch as a carbon source. *Journal of Bioscience and Bioengineering*, 93(3), 303–308. [https://doi.org/10.1016/S1389-1723\(02\)80032-9](https://doi.org/10.1016/S1389-1723(02)80032-9)
- Kinzelbach, W., Schäfer, W., & Herzer, J. (1991). Numerical modeling of natural and enhanced denitrification processes in aquifers. *Water Resources Research*, 27(6), 1123–1135. <https://doi.org/10.1029/91WR00474>
- Kool, D. M., Wrage, N., Oenema, O., Dolfing, J., & Van Groenigen, J. W. (2007). Oxygen exchange between (de) nitrification intermediates and  $\text{H}_2\text{O}$  and its implications for source determination of  $\text{NO}_3$  and  $\text{N}_2\text{O}$ : A review. *Rapid Communications in Mass Spectrometry: Rapid Communications in Mass Spectrometry*, 21(22), 3569–3578. <https://doi.org/10.1002/rcm>
- Kraft, B., Strous, M., & Tegetmeyer, H. E. (2011). Microbial nitrate respiration—Genes, enzymes and environmental distribution. *Journal of Biotechnology*, 155(1), 104–117. <https://doi.org/10.1016/j.jbiotec.2010.12.025>

- Li, Y., Zhu, G., Ng, W. J., & Tan, S. K. (2014). A review on removing pharmaceutical contaminants from wastewater by constructed wetlands: Design, performance and mechanism. *Science of the Total Environment*, 468–469, 908–932. <https://doi.org/10.1016/j.scitotenv.2013.09.018>
- Liu, F., Huang, G., Fallowfield, H., Guan, H., Zhu, L., & Hu, H. (2013). *Study on heterotrophic-autotrophic denitrification permeable reactive barriers (HAD PRBs) for in situ groundwater remediation*. Springer Science & Business Media.
- Lu, S., Zhang, P., Jin, X., Xiang, C., Gui, M., Zhang, J., & Li, F. (2009). Nitrogen removal from agricultural run-off by full-scale constructed wetland in China. *Hydrobiologia*, 621(1), 115–126. <https://doi.org/10.1007/s10750-008-9636-1>
- Maggi, F., & Riley, W. J. (2009). Transient competitive complexation in biological kinetic isotope fractionation explains nonsteady isotopic effects: Theory and application to denitrification in soils. *Journal of Geophysical Research*, 114(G4), G04012. <https://doi.org/10.1029/2008JG000878>
- Maggi, F., & Riley, W. J. (2010). Mathematical treatment of isotopologue and isotopomer speciation and fractionation in biochemical kinetics. *Geochimica et Cosmochimica Acta*, 74(6), 1823–1835. <https://doi.org/10.1016/j.gca.2009.12.021>
- Margalef-Martí, R., Carrey, R., Merchán, D., Soler, A., Causapé, J., & Otero, N. (2019). Feasibility of using rural waste products to increase the denitrification efficiency in a surface flow constructed wetland. *Journal of Hydrology*, 578, 124035. <https://doi.org/10.1016/j.jhydrol.2019.124035>
- Margalef-Martí, R., Carrey, R., Soler, A., & Otero, N. (2019). Evaluating the potential use of a dairy industry residue to induce denitrification in polluted water bodies: A flow-through experiment. *Journal of Environmental Management*, 245, 86–94. <https://doi.org/10.1016/j.jenvman.2019.03.086>
- Mariotti, A., Germon, J. C., Hubert, P., Kaiser, P., Letolle, R., Tardieux, A., & Tardieux, P. (1981). Experimental determination of nitrogen kinetic isotope fractionation: Some principles; illustration for the denitrification and nitrification processes. *Plant and Soil*, 62(3), 413–430. <https://doi.org/10.1007/BF02374138>
- Mariotti, A., Landreau, A., & Simon, B. (1988). <sup>15</sup>N isotope biogeochemistry and natural denitrification process in groundwater: Application to the chalk aquifer of northern France. *Geochimica et Cosmochimica Acta*, 52(7), 1869–1878. [https://doi.org/10.1016/0016-7037\(88\)90010-5](https://doi.org/10.1016/0016-7037(88)90010-5)
- Mastrocicco, M., Colombani, N., Salemi, E., & Castaldelli, G. (2011). Reactive modeling of denitrification in soils with natural and depleted organic matter. *Water, Air, and Soil Pollution*, 222(1–4), 205–215. <https://doi.org/10.1007/s11270-011-0817-6>
- McIlvin, M. R., & Altabet, M. A. (2005). Chemical conversion of nitrate and nitrite to nitrous oxide for nitrogen and oxygen isotopic analysis in freshwater and seawater. *Analytical Chemistry*, 77(17), 5589–5595. <https://doi.org/10.1021/ac050528s>
- Merchán, D., Causapé, J., Abrahão, R., & García-Garizábal, I. (2015). Assessment of a newly implemented irrigated area (Lerma Basin, Spain) over a 10-year period. I: Water balances and irrigation performance. *Agricultural Water Management*, 158, 277–287. <https://doi.org/10.1016/j.agwat.2015.04.016>
- Nardi, A., & de Vries, L. M. (2017). GibbsStudio, Barcelona science technologies SL. Retrieved from <https://gibbsstudio.io/>
- Niculescu, V. C., & Ionete, R. E. (2023). An overview on management and valorisation of winery wastes. *Applied Sciences*, 13(8), 5063. <https://doi.org/10.3390/app13085063>
- Oliveira, C. P., Beatriz, A., Gloria, M., Barbour, J. F., & Scanlan, A. R. (2002). Nitrate, nitrite, and volatile nitrosamines in whey-containing food products. *Journal of Agricultural and Food Chemistry*, 43(4), 967–969. <https://doi.org/10.1021/jf00052a023>
- Otero, N., Torrentó, C., Soler, A., Menció, A., & Mas-Pla, J. (2009). Monitoring groundwater nitrate attenuation in a regional system coupling hydrogeology with multi-isotopic methods: The case of Plana de Vic (Osona, Spain). *Agriculture, Ecosystems & Environment*, 133(1–2), 103–113. <https://doi.org/10.1016/j.agee.2009.05.007>
- Parkhurst, D. L., & Appelo, C. A. J. (2013). Description of input and examples for PHREEQC version 3—A computer program for speciation, batch-reaction, one-dimensional transport, and inverse geochemical calculations. In *U.S. Geological Survey Techniques and Methods* (Vol. 6, pp. 6–43A). Chapter A43. [https://doi.org/10.1016/0029-6554\(94\)90020-5](https://doi.org/10.1016/0029-6554(94)90020-5)
- Phipps, R. G., & Crumpton, W. G. (1994). Factors affecting nitrogen loss in experimental wetlands with different hydrologic loads. *Ecological Engineering*, 3(4), 399–408. [https://doi.org/10.1016/0925-8574\(94\)00009-3](https://doi.org/10.1016/0925-8574(94)00009-3)
- Picardal, F. (2012). Abiotic and microbial interactions during anaerobic transformations of Fe(II) and NO<sub>x</sub><sup>-</sup>. *Frontiers in Microbiology*, 3, 1–7. <https://doi.org/10.3389/fmicb.2012.00112>
- Rodríguez-Escales, P., Breukelen, B. M. V., Vidal-gavilan, G., Soler, A., & Folch, A. (2014). Integrated modeling of biogeochemical reactions and associated isotope fractionations at batch scale: A tool to monitor enhanced biodenitrification applications. *Chemical Geology*, 365, 20–29. <https://doi.org/10.1016/j.chemgeo.2013.12.003>
- Rodríguez-Escales, P., Folch, A., van Breukelen, B. M., Vidal-Gavilan, G., & Sanchez-Vila, X. (2016). Modeling long term Enhanced in situ Biodenitrification and induced heterogeneity in column experiments under different feeding strategies. *Journal of Hydrology*, 538, 127–137. <https://doi.org/10.1016/j.jhydrol.2016.04.012>
- Ryabenko, E., Altabet, M. A., & Wallace, D. W. R. (2009). Effect of chloride on the chemical conversion of nitrate to nitrous oxide for δ<sup>15</sup>N analysis. *Limnology and Oceanography: Methods*, 7(7), 545–552. <https://doi.org/10.4319/lom.2009.7.545>
- Saeed, T., & Sun, G. (2017). A comprehensive review on nutrients and organics removal from different wastewaters employing subsurface flow constructed wetlands. *Critical Reviews in Environmental Science and Technology*, 47(4), 203–288. <https://doi.org/10.1080/10643389.2017.1318615>
- Sebilo, M., Aloisi, G., Mayer, B., Perrin, E., Vaury, V., Mothet, A., & Laverman, A. M. (2019). Controls on the isotopic composition of nitrite (δ<sup>15</sup>N and δ<sup>18</sup>O) during denitrification in freshwater sediments. *Scientific Reports*, 9(1), 1–14. <https://doi.org/10.1038/s41598-019-54014-3>
- Sebilo, M., Billen, G., Mayer, B., Billioud, D., Grably, M., Garnier, J., & Mariotti, A. (2006). Assessing nitrification and denitrification in the Seine River and estuary using chemical and isotopic techniques. *Ecosystems*, 9(4), 564–577. <https://doi.org/10.1007/s10021-006-0151-9>
- Seifert, D., & Engesgaard, P. (2007). Use of tracer tests to investigate changes in flow and transport properties due to bioclogging of porous media. *Journal of Contaminant Hydrology*, 93(1–4), 58–71. <https://doi.org/10.1016/j.jconhyd.2007.01.014>
- Singleton, M. J., Esser, B. K., Moran, J. E., Hudson, G. B., Menab, W. W., & Harter, T. (2007). Saturated zone denitrification: Potential for natural attenuation of nitrate contamination in shallow groundwater under dairy operations. *Environmental Science and Technology*, 41(3), 759–765. <https://doi.org/10.1021/es061253g>
- Torrijos, V., Gonzalo, O. G., Trueba-Santiso, A., Ruiz, I., & Soto, M. (2016). Effect of by-pass and effluent recirculation on nitrogen removal in hybrid constructed wetlands for domestic and industrial wastewater treatment. *Water Research*, 103, 92–100. <https://doi.org/10.1016/j.watres.2016.07.028>
- United Nations. (2022). *The Sustainable Development Goals Report 2022*. United Nations Publication Issued by the Department of Economic and Social Affairs. Retrieved from <https://unstats.un.org/sdgs/report/2022/>
- Valhondo, C., Martínez-Landa, L., Carrera, J., Díaz-Cruz, S. M., Amalfitano, S., & Levantesi, C. (2020). Six artificial recharge pilot replicates to gain insight into water quality enhancement processes. *Chemosphere*, 240, 124826. <https://doi.org/10.1016/j.chemosphere.2019.124826>

- Van Breukelen, B. M., & Prommer, H. (2008). Beyond the Rayleigh equation: Reactive transport modeling of isotope fractionation effects to improve quantification of biodegradation. *Environmental Science and Technology*, *42*(7), 2457–2463. <https://doi.org/10.1021/es071981j>
- WHO. (2017). Guidelines for drinking-water quality: Fourth edition incorporating the first addendum. *Guidelines for drinking-water quality: Fourth edition incorporating the first addendum* (Vol. 541). Retrieved from <https://apps.who.int/iris/bitstream/handle/10665/254637/9789241549950-eng.pdf;jsessionid=C9942C5DBCC2BDC53A892D79B3844EE8?sequence=1%0A>; <http://www.ncbi.nlm.nih.gov/pubmed/28759192>
- Wu, S., Kusch, P., Brix, H., Vymazal, J., & Dong, R. (2014). Development of constructed wetlands in performance intensifications for wastewater treatment: A nitrogen and organic matter targeted review. *Water Research*, *57*, 40–55. <https://doi.org/10.1016/j.watres.2014.03.020>
- Wunderlich, A., Meckenstock, R. U., & Einsiedl, F. (2013). A mixture of nitrite-oxidizing and denitrifying microorganisms affects the  $\delta^{18}\text{O}$  of dissolved nitrate during anaerobic microbial denitrification depending on the  $\delta^{18}\text{O}$  of ambient water. *Geochimica et Cosmochimica Acta*, *119*, 31–45. <https://doi.org/10.1016/j.gca.2013.05.028>
- Zhu, C. (2012). Geochemical modeling in environmental and geological studies. In *Encyclopedia of Sustainability Science and Technology* (pp. 4094–4104). <https://doi.org/10.1007/978-1-4419-0851-3>